Bulletin of the New Zealand Society for Earthquake Engineering, Vol. 52, No. 4, December 2019

GROUND MOTION SIMULATIONS OF HOPE FAULT EARTHQUAKES

Ethan M. Thomson[1], Robin L. Lee[2] and Brendon A. Bradley[3]

(Submitted *May 2019*; Reviewed *July 2019*; Accepted *October 2019*)

ABSTRACT

This paper examines ground motions for a major potential M_w7.51 rupture of the Hope Fault using a physics-based simulation methodology and a 3D crustal velocity model of New Zealand. The simulation methodology was validated for use in the region through comparison with observations for a suite of historic small magnitude earthquakes located proximal to the Hope Fault. Simulations are compared with conventionally utilised empirical ground motion models, with simulated peak ground velocities being notably higher in regions with modelled sedimentary basins. A sensitivity analysis was undertaken where the source characteristics of magnitude, stress parameter, hypocentre location and kinematic slip distribution were varied and an analysis of their effect on ground motion intensities is presented. It was found that the magnitude and stress parameter strongly influenced long and short period ground motion amplitudes, respectively. Ground motion intensities for the Hope Fault scenario are compared with the 2016 Kaikōura M_w7.8 earthquake, it was found that the Kaikōura earthquake produced stronger motions along the eastern South Island, while the Hope Fault scenario resulted in stronger motions immediately West of the near-fault region and similar levels of ground motion in Canterbury. The simulated ground motions for this scenario complement prior empirically-based estimates and are informative for mitigation and emergency planning purposes

INTRODUCTION

The 2016 Kaikōura M_w7.8 earthquake resulted in significant ground motions and caused substantial damage to infrastructure throughout the Northern South Island and as far away as Wellington [1, 2], and provides motivation for further assessment of the potential impacts from significant ruptures of faults in this region of New Zealand.

The Hope Fault is generally considered as a collection of contiguous faults in the South Island of New Zealand and can be traced from the Alpine Fault to offshore northeast of Kaikōura [3, 4]. Due to its high slip rate (up to $23mm/yr$, Langridge *et al.* [4]), and potential to produce large-to-great earthquake magnitudes, it poses a significant hazard to critical infrastructure (e.g. telecommunications, electricity, road) and urban populations in the South Island.

Understanding the South Island-impacts of a major Hope Fault earthquake can be advanced through improved prediction of earthquake-induced ground motions via recently developed physics-based methods (e.g. [5]). Such methods are able to explicitly model directivity-basin coupling, basin-generated surface waves and near-surface site response, which are implicitly modelled in conventional empirical ground motion models based on ergodic global averages.

Leveraging physics-based ground motion simulation advancements and validation, this paper presents physics-based ground motion simulations for a M_w7.51 Hope Fault scenario. We first present the salient features of the Hope Fault system and scenario rupture modelled, as well as the 3D crustal model for the region. Secondly, we discuss the adopted ground motion simulation method, prior validation, as well as as additional validation we performed for small magnitude earthquakes located proximal to the Hope Fault system. Thirdly, we discuss simulations of ground motion scenario ruptures, sensitivities, and comparisons to empirical models. Finally, we discuss the simulation results for the Hope Fault scenarios in the context of the ground shaking from the recent 2016 Kaikōura earthquake.

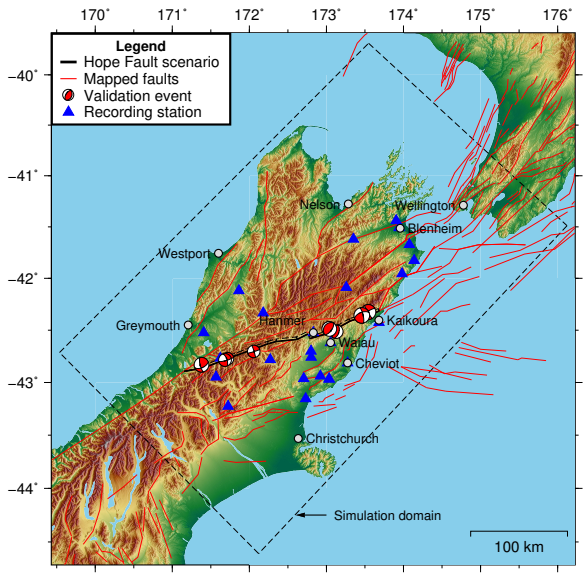

Figure 1: Study region illustrating mapped faults [6] in New Zealand and the Hope Fault scenario utilised in this study. The locations of instrumentally-recorded historic earthquakes and strong motion stations utilised to validate the simulation methodology (see Validation Using Historic Earthquakes) are also shown.

[1] *PhD Candidate, University of Canterbury, Christchurch*
[2] *Corresponding Author, Postdoctoral Fellow, University of Canterbury, Christchurch, robin.lee@canterbury.ac.nz*
[3] *Professor, University of Canterbury, Christchurch (Member)*

THE HOPE FAULT AND REGIONAL SETTING

Hope Fault Rupture Scenario

As illustrated in Figure 1, the Hope Fault system is a set of near-contiguous dextral-slip faults in the South Island of New Zealand, and can be traced from the Alpine Fault to offshore Northeast of Kaikōura [3, 4]. Significant ruptures have occurred during New Zealand's historic period ($150yr$): the 1888 $M7-7.3$ North Canterbury earthquake ruptured a $30km$ segment of the Hope Fault [7], while the 2016 Kaikōura earthquake is inferred to have potentially involved seaward sections of the Hope Fault [2]. However, the majority of segments have not ruptured coseismically within New Zealand's short historic period [4, 8, 9].

Previous studies have detailed the geomorphology of the segments comprising the Hope Fault system. From West to East, the major segments are named as the Kelly, Taramakau, Hurunui, Hope River, Conway and Seaward (see [4, 8, 9, 11, 12]). Characteristic ruptures of individual Hope Fault segments have been investigated as part of the New Zealand National Seismic Hazard Model (NSHM) [6], however, as these discrete fault segments are the result of modelling assumptions, it is unlikely that a rupture on the Hope Fault system will respect these segment boundaries (e.g. [13, 14]). No previous studies have comprehensively assessed the ground motions resulting from a simultaneous rupture of multiple Hope Fault segments, therefore, there is a need to investigate ground motions from a potential large ($M_w > 7$) Hope Fault earthquake.

Numerous segments of the Hope Fault as represented in the NSHM were combined to form a composite rupture scenario. Figure 1 presents the geometry of the Hope Fault rupture planes and their location within the South Island of New Zealand. In the West of the Hope Fault system there is a junction at the segment boundary between the Hurunui, Taramakau and Kelly segments, the adopted scenario omits the Taramakau segment in favour of Kelly, which branches onto the Hurunui, as this is expected, from the perspective of continuity of strike direction, and thus rupture dynamics, to be the more probable scenario (J. Pettinga, personal communication). At the Western end of the scenario the rupture terminates on the Kelly Fault and is assumed not to progress onto the adjacent Alpine Fault.

The rupture scenario consists of two contiguous fault planes separated with a stepover (which is $6km$ at the ground surface) at the Hanmer basin. While previous thinking has conventionally considered that stepovers of this size would cause termination of rupture propagation [15], numerous international earthquakes indicate significant 'rupture jumping' (e.g. [16, 17]), notably, the 2016 Kaikōura earthquake illustrated that ruptures are able to propagate through stepovers which have a surface separation of $15-20km$ length (albeit less at seismogenic depths). Therefore, the stepover at the Hanmer basin does not exclude the possibility of a rupture continuing through this geometrical complexity (J. Pettinga, personal communication), and hence was considered.

In the East of the Hope Fault system at Kaikōura there is a junction between the Conway Onshore and Offshore segments and the Jordan Thrust. The Conway Offshore segment has a relatively low slip rate compared with the Onshore segment, partially due to the slip transfer onto the Jordan Thrust. This indicates that the Conway offshore segment is unlikely to participate in the majority of large Hope Fault earthquakes and therefore was not included in the rupture scenario generated. Some segments of the Jordan Thrust are inferred to have participated in the 2016 Kaikōura earthquake [2, 18]. Given the recent stress release, combined with the difference in faulting mechanism, it was deemed unlikely that rupture would propagate onto the Jordan Thrust in the next event and therefore, the constructed scenario terminates at the Eastern end of the Conway segment.

In summary, the adopted scenario involves four fault planes for a total along-strike length of $219km$ with dip varying between 80 and 90 degrees for the various planes (as noted in [6]). Stirling *et al.* [6] considers the seismogenic depth of these segments to be $12km$, based on background seismicity, however research (e.g. [19]) indicates that ruptures beyond the seismogenic depth are probable for large earthquakes. On this basis, prior ground motion studies (e.g. [20, 21]) have adopted a lower seismogenic depth of $15km$, in which the mean slip amplitudes linearly taper toward zero over the lower $3km$ depth. The total rupture area of the modelled faults is therefore $3323km^2$ yielding a mean characteristic magnitude of

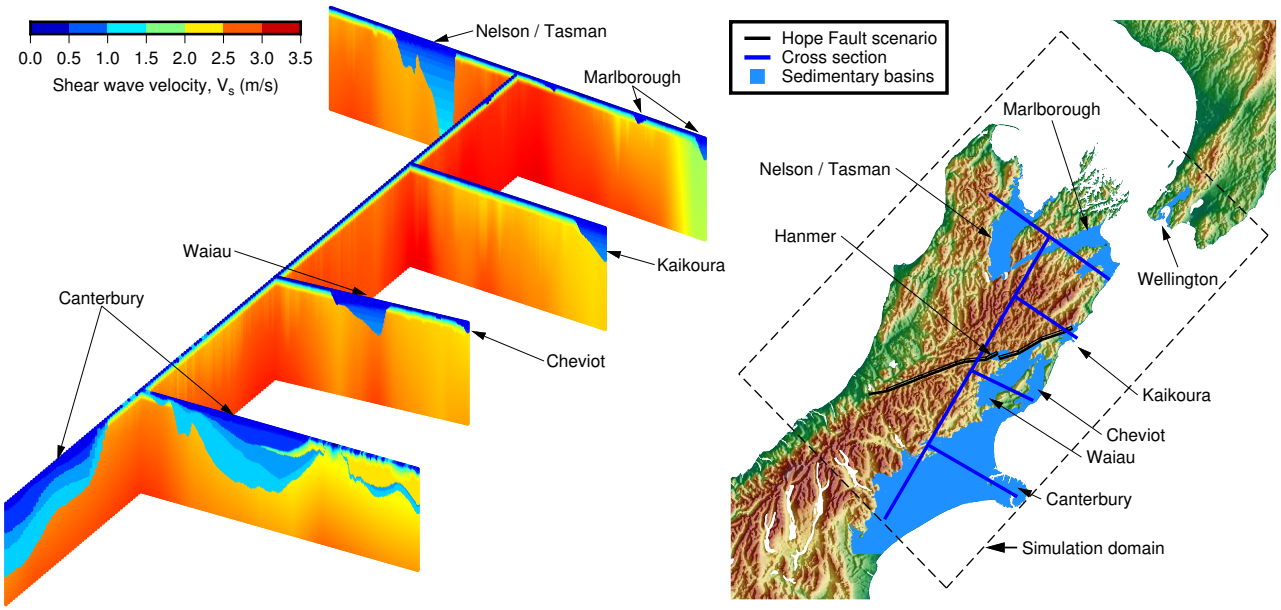

Figure 2: Crustal modelling in the region of interest using the NZVM [10], illustrating the location of the Hope Fault rupture scenario, explicitly modelled basins, and illustrative S-wave velocity cross sections through basins.

$M_w = 7.51$ using the preferred Leonard [22] magnitude scaling relation (see Bradley *et al.* [21] for a discussion on appropriate scaling relations for use in ground motions simulation applications). Further details of the kinematic rupture prescription are presented in Rupture Kinematics. Only characteristic ruptures of the adopted geometry were considered as this study intends to present ground motions from a major Hope Fault scenario, and not to exhaustively investigate ground motions from all potential scenarios involving different segments of the Hope Fault system, or all other potential ruptures in the region. In this regard we refer readers to Tarbali *et al.* [23] and Graves *et al.* [24] for the use of ground motion simulations in probabilistic seismic hazard analysis.

3D Crustal Model of the Region

In order to perform realistic ground motion simulations it is critical to utilise a 3D crustal model that provides an accurate representation of the regional velocity (P-wave, S-wave) and density structure. A critical component in such models is the characterisation of sedimentary basins which are a controlling factor in modelling ground motion amplitudes and basin-generated surface waves of engineering interest. The recently developed New Zealand Velocity Model (NZVM) of Thomson *et al.* [10] explicitly models numerous sedimentary basins in the region of interest, and was adopted for this study. Note that the NZVM does not characterise all of New Zealand's sedimentary basins, as priority was given to modelling basins with greater population density, or locations with strong motion instruments (important for validation). As a result, simulated ground motion amplitudes have a spatially-variable accuracy and precision. Figure 2 presents S-wave velocity transects through the NZVM illustrating the relatively low velocities within the characterised sedimentary basins (Canterbury, Waiau, Cheviot, Hanmer, Kaikōura, Nelson / Tasman, Marlborough and Wellington).

The NZVM has been extensively utilised to perform ground motion simulations of historical and potential future earthquakes in New Zealand. Lee *et al.* [25] conducted ground motion simulations of 148 historic small-to-moderate magnitude $3.5 \leq M_w \leq 5$ earthquakes in an extensive validation exercise. Bradley *et al.* [26] simulated 10 events from the 2010-2011 Canterbury earthquakes sequence while Razafindrakoto *et al.* [27] focussed on simulating the 2011 M_w6.2 Christchurch earthquake from the same sequence and Bradley *et al.* [1] simulated motions for the 2016 M_w7.8 Kaikōura earthquake. Bradley *et al.* [21] simulated a M_w7.9 scenario rupture of Alpine Fault, while Tarbali *et al.* [23] simulated characteristic ruptures of seismic sources in the NSHM to perform a New Zealand-wide probabilistic seismic hazard analysis with the NZVM.

GROUND MOTION SIMULATION METHODOLOGY AND VALIDATION

Methodology

The Graves and Pitarka [5, 20, 28] hybrid broadband ground motion simulation methodology was used to simulate scenario Hope Fault ruptures. The low frequency (LF, $f < 1Hz$) portion of the methodology utilises a comprehensive physics-based finite-difference algorithm to simulate viscoelastic wave propagation within a 3D crustal model. The high frequency (HF, $f > 1Hz$) portion of the methodology uses a simplified physics-based approach which constructs a time-series from the summation of multiple stochastic source sub-faults and a simple 1D velocity model, to which a V_{s30}-based site amplification is then applied [29]. For this study, the New Zealand-specific V_{s30} model of Foster *et al.* [30] was adopted. The LF and HF simulations are then merged [5] to form a site-specific broadband ($f = 0 - 50Hz$) time-series, from which spectral ordinates over the range $T = 0 - 10s$ can be reliably derived [31]. The methodology has significant conceptual advantages over conventional empirical modelling techniques as discussed further in Bradley [32].

The Graves and Pitarka [5] ground motion simulation methodology has been extensively applied internationally to simulate historic (e.g. the 1989 Loma Prieta earthquake in Northern California [33]) and scenario earthquakes (e.g. a San Andreas rupture scenario in Southern California [34]). In addition to international applications, the methodology has been utilised to simulate scenario and historic earthquakes in New Zealand (as presented in 3D Crustal Model of the Region). The recent applications of the methodology to simulating ground motions in New Zealand enable the methodology to be applied with confidence in simulation scenario ruptures of the Hope Fault.

Validation Using Historic Earthquakes

Validation of ground motion simulation methods is critical to develop confidence in their predictive capabilities before they are used in forward prediction of future events [32]. It is also important to note that region-specific validation is required in order to ascertain the appropriateness of the simulation methodology and 3D crustal velocity model [35]. Ideally, the validation would consist of comparing simulations against observations for earthquakes that have similar characteristics to the prospective earthquake and have occurred in the same geographic region of interest. However, large magnitude earthquakes similar to the Hope Fault rupture scenario considered in this study have not been observed in the instrumented period. Therefore small-to-moderate magnitude historic earthquakes records are utilised to validate the region specific application, and the findings extrapolated for larger magnitude earthquakes. It is noted that the ground motion amplitudes from such small magnitude validation events will not induce non-linear site effects that will manifest at some locations during strong ground motions in larger magnitude events.

Several recent validation studies have used small magnitude earthquakes (e.g. [25, 36]) to validate ground motion simulation methodologies and crustal velocity models. The obvious advantage of small magnitude earthquakes is that they occur much more frequently than large magnitude earthquakes. Furthermore, since kinematic simulations of finite faults are essentially a summation of subfault ruptures, the validation of small magnitude events provides some merit for large magnitude events as well. Therefore, region-specific validation using small magnitude earthquakes in the Hope Fault region was conducted.

In addition to the comparison between simulations and observations, a parallel comparison between empirically predicted intensity measures and observations is also carried out to provide a benchmark corresponding to conventional ground motion estimation techniques. This study considers pseudo-spectral accelerations using the Bradley [37] New Zealand-specific ground motion model (GMM).

A dataset of nine small magnitude ($4.0 \leq Mw \leq 5.0$) historic earthquakes located proximal to the Hope Fault (as shown in Figure 1) were considered for this validation study. From these earthquakes, 53 high-quality ground motions were recorded across 25 different strong motion stations throughout the region.

The quality of the observed ground motions were determined using a ground motion quality classification neural network [38]. Recorded ground motions were processed with a low-pass causal Butterworth filter of 50Hz, with a corner frequency of 0.05Hz for high-pass filter. This filtering yields a groundmotion that can produce spectral ordinates over the range $T = 0.01 - 10s$.

The ground motion predictions are compared against observations through natural logarithm residuals of intensity measures:

$$\Delta = ln(IM_{obs}) - ln(IM_{pred})$$

where Δ is the total residual, IM_{obs} is the observed intensity measure, and IM_{pred} is the predicted IM, either from simulation or empirical prediction. A positive total residual would indicate underprediction while a negative total residual would indicate overprediction. The model bias is subsequently calculated as the average of all total residuals associated with each ground motion record and represents the systematic difference between observation and prediction.

Figure 3 presents the total residuals for the physics-based simulations and empirical GMMs. Sites are separated into two groups: soil sites in modelled basins; and rock and non-basin sites. At short vibration periods ($T < 0.2s$) the simulation has less bias than the empirical prediction for both site groupings; at moderate periods ($T = 0.3 - 1.0s$) the empirical prediction has less bias; and at longer periods ($T = 1 - 5s$) the predictions (for both empirical and simulation) are approximately unbiased for basin sites, but biased for non-basin sites to a similar extent for both empirical and simulation predictions. Across all intensity measures considered, the total residual standard deviations are similar for both methods. Overall, the size of the model biases for simulation and empirical prediction are relatively similar where they are less than 1 for all spectral intensity measures considered.

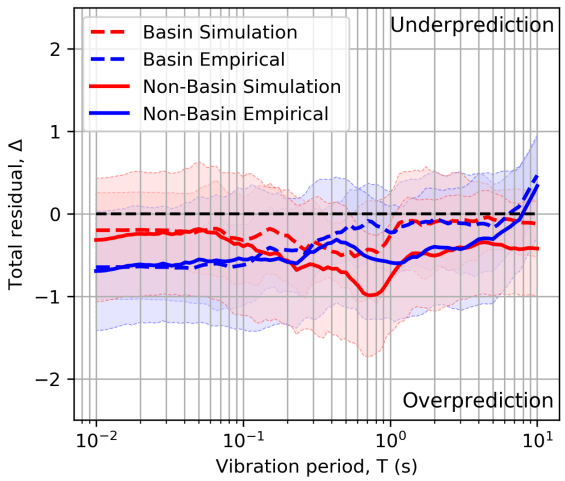

Figure 3: Total residuals between observed and predicted (simulated and empirical) intensity measures for 53 ground motion records, from nine validation events, recorded at 25 unique strong motion stations. Residuals are grouped into stations located in basin or non-basin sites. Lines indicate the mean residual and the shaded regions plus or minus one standard deviation range.

Ultimately, this validation exercise indicates that the physics-based simulations are generally comparable to empirical ground motion models for small magnitude earthquakes in the Hope Fault region. Although the number of ground motion records considered and number of historic events utilised limits robust statistical inferences, the goal was not to present a comprehensive validation of the simulations. The purpose of the validation was to assess how the simulation methodology performed relative to the empirical prediction. Therefore, the comparable performance suggests that the simulation methodology and crustal velocity model employed are appropriate for Hope Fault scenario rupture simulations and provide predictive insight.

SIMULATED GROUND MOTION INTENSITIES

To investigate ground motion intensities which can occur from a Hope Fault rupture, several realisations of the kinematic source model are simulated. However, to quantify the effect of each realisation, a reference simulation needs to be established corresponding to a baseline 'median' scenario. This section firstly provides details of the reference scenario simulation and associated intensity measures, followed by a subsequent examination of simulation sensitivity to modelling parameter uncertainty. Finally, the spatial variation of ground motion intensity from a Hope Fault scenario is compared with the 2016 Kaikōura earthquake.

Reference Simulation

Simulation Computational Details

The reference simulation utilised a 3D finite difference grid with horizontal dimensions of $296.3 \times 475.5km$ (shown in Figure 1) adopted to capture ground motion intensities in urban regions at large source-to-site distances, extending to a depth of $Z_{max} = 47km$ with a $0.1km$ grid spacing (thus a total of 6.60 billion spatial grid points in the domain) with material properties from the NZVM [10]. A squashed topographic representation (see [10]) was utilised and is illustrated in Figure 2. The simulation duration was set at $t_{end} = 180s$ with a timestep of $\Delta t = 0.005s$ (i.e. 36,000 time steps) and a minimum shear-wave velocity of $V_{s,min} = 500m/s$ enabling the LF simulation to accurately resolve $f \leq 1Hz$. Simulations were conducted on the NeSI Maui HPC (see Data and Resources) utilising 1840 compute cores with a typical simulation taking $7.5 - 8.0$ hours of wall clock time. To reduce storage requirements, surficial ground motion time-series were only stored on a uniform grid with $500m$ spacing for post processing.

Rupture Kinematics

The kinematic source model used for the reference scenario adopts the fault geometry previously discussed in Hope Fault Rupture Scenario. The kinematic source representation for the Hope Fault reference scenario was generated utilising the Graves and Pitarka [5] methodology, which uses a spatial field model to develop representations of slip, rake and rise time. Figure 4 illustrates the variation of slip amplitude, rise time and rake direction over the rupture. The four fault planes were specified for rupture generation and appropriate delays were set such that a rupture propagating to the end of a segment will kinematically 'trigger' rupture on the next, the same method was used to trigger ruptures on the adjacent segments at Hanmer Basin step over (see [1] as another example of this assumption). The hypocentre location is denoted by a red star in the slip amplitude panel (top row of Figure 4), with the bilateral rupture propagation illustrated by contours indicating the temporal evolution of slip.

Ground Motion Intensities for the Reference Simulation

Figure 5 presents instantaneous particle velocities at the ground surface for three time instances ($t = 15s, 30s$ and $50s$) for the Hope Fault reference simulation. The bilateral rupture and wave

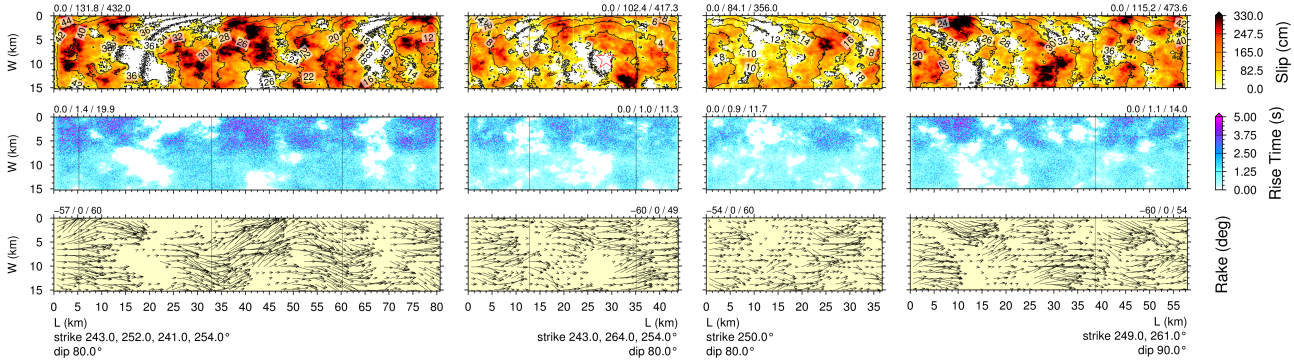

Figure 4: Illustration of slip amplitude (top row), rise time (middle) and rake direction (bottom row) of the Hope Fault reference rupture scenario. The four segments are discussed in Hope Fault Rupture Scenario. The numbers above each segment represent the minimium/mean/maximum of the quantity depicted.

propagation associated with the central location of the hypocentre can be clearly seen as the wavefronts propagate both East and West along the fault trace. In Figure 5c large velocity amplitudes resulting from basin amplification can be identified in the some of the NZVM sedimentary basins (see Figure 2). (A link to the 3D visualisation of the Hope Fault reference simulation can found in Data and Resources).

Figure 6 presents intensity measure plots for the Hope Fault reference scenario for PGV, D_{s5-95}, pSA(0.5s) and pSA(3.0s). It can be seen that the peak ground velocity (PGV; Figure 6a) is relatively high in the sedimentary basins (see Figure 2) with small source-to-site distances (e.g. Hanmer, Waiau, Cheviot and Kaikōura) while basin amplification is less prominent, although still evident, in the basins with relatively large source-to-site distances (e.g. Nelson, Marlborough and Christchurch). The nature of the bilateral rupture (Figure 5) leads to smaller relative $5-95\%$ significant durations (D_{s5-95}; Figure 6b) (for a given source-to-site distance) as a result of rupture directivity. Locations perpendicular to the rupture strike direction, in regions of neutral directivity, have a longer significant duration, which are further increased if they lie within deep sedimentary basins (e.g. Canterbury).

The spatial distribution of pSA(0.5s) and pSA(3.0s) amplitudes in Figure 6c and Figure 6d, respectively, both show general reductions with source-to-site distance. The effect of sedimentary basins is larger for pSA(3.0s) amplitudes relative to pSA(0.5s) amplitudes. It is also worth noting that given the LF to HF transition frequency of $f = 1Hz$, the pSA(0.5s) amplitudes are dominated by the (simplified-physics) HF component which doesn't comprehensively model the basins as opposed to the pSA(3.0s) being dominated by the (comprehensive physics) LF component. (PGA for the reference simulation can be viewed in the appendix).

Comparison with Empirical Ground Motion Estimates

Figure 7 presents empirical estimates for PGV, D_{s5-95}, pSA(0.5s) and pSA(3.0s) using the Afshari and Stewart [39] (for D_{s5-95}) and Bradley [37] (for PGV, pSA(0.5s) and pSA(3.0s)) models (in combination with the Foster *et al.* [30] New Zealand V_{s30} model and correlations to derive other necessary inputs, e.g. $Z_{1.0}$). As the empirical models vary primarily with source-to-site distance (R_{rup}) for a given rupture (in a similar way to the HF simulation methodology), the predicted intensity measures from empirical models exhibit a near-elliptical variation about the rupture plane. The principal reason for the localised deviations from a simple source-to-site distance decay is the local site response associated with the spatial variation in V_{s30} (via the New Zealand-specific model of Foster *et al.* [30] as noted in Methodology). This is in contrast to simulation-derived intensity measures (see Figure 6), that exhibit a more complex spatial variation.

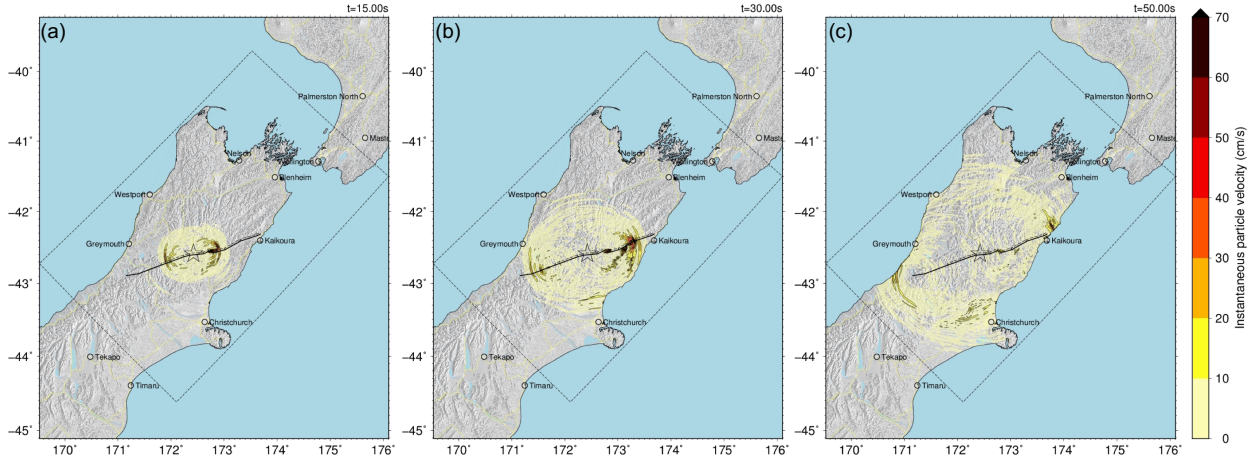

Figure 5: Instantaneous particle velocities (vector maximum in the horizontal plane) for the Hope Fault reference scenario: (a) t=15s; (b) t=30s; and (c) t=50s. The figures collectively illustrate bilateral rupture propagation, wave propagation and reverberation within the Hanmer, Cheviot, Waiau and Canterbury sedimentary basins. (A link to a 3D visualisation of the simulation can found in Data and Resources)

Figure 8 presents ratios of empirical and simulation intensity measures for the Hope Fault reference scenario. The ratio metric is $R_{IM} = \ln(IM_{emp}/IM_{sim})$ (or $R = \ln(emp/sim)$ for brevity) such that $R > 0$ indicates empirical predictions greater than the reference simulation and vice versa for $R < 0$. As the simulation pSA(0.5s) is dominated by the HF component, and this is similar to empirical models in terms of source-to-site distance, attenuation and V_{s30}-based site effects, the similarities are apparent in the pSA(0.5s) ratio shown in Figure 8c. Figure 8b clearly show the directivity related influence on D_{s5-95}, as forward directivity dominated areas have $R_{D_{s5-95}} > 0$ and neutral directivity areas have $R_{D_{s5-95}} < 0$. Figure 8a and Figure 8d illustrate the significant impact of sedimentary basins on simulation derived PGV and pSA(3.0s), respectively.

In order to provide further insight into the spatial trends in Figure 8, Figure 9 presents a comparison of simulation and empirical estimates for PGV, D_{s5-95}, pSA(0.5s) and pSA(3.0s) as a function of source-to-site distance (R_{rup}). The errorbars for the simulation were derived from the binned average value of all sites within the simulation domain and the height of the bar represents one standard deviation, while the empirical median was similarly derived from the binned average value of empirical estimates at the locations predicted. Figure 9c illustrates the pSA(0.5s) for the simulation is generally higher for $10 < R_{rup} < 100km$, a trend that is spatially apparent in Figure 8c. In Figure 9c the spatial directivity trend that was apparent in Figure 8b is removed and the median simulation and empirical significant duration is broadly consistent for

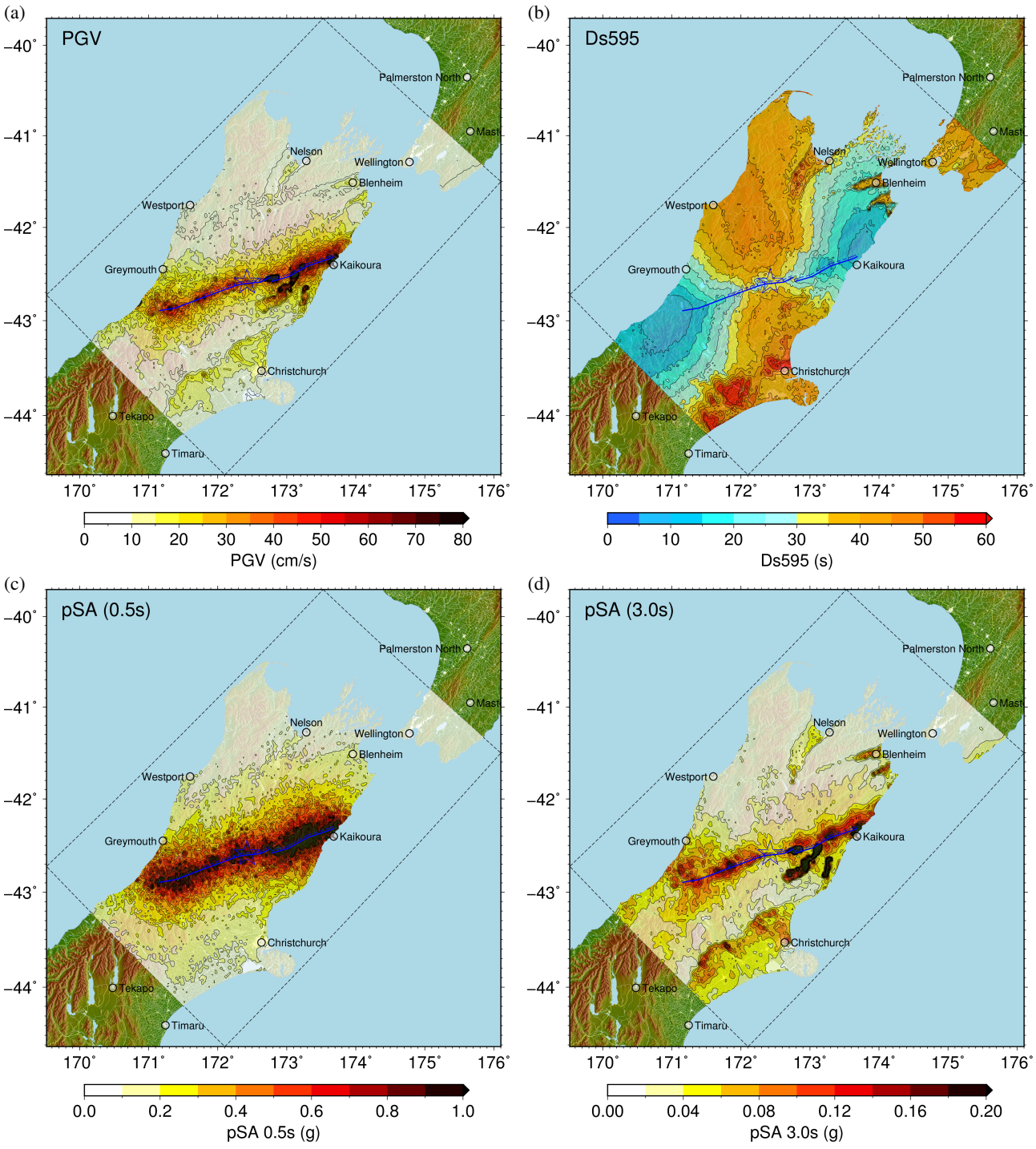

Figure 6: Simulated intensity measures for the Hope Fault reference scenario: (a) PGV; (b) D_{s5-95}; (c) pSA(0.5s); and (d) pSA(3.0s).

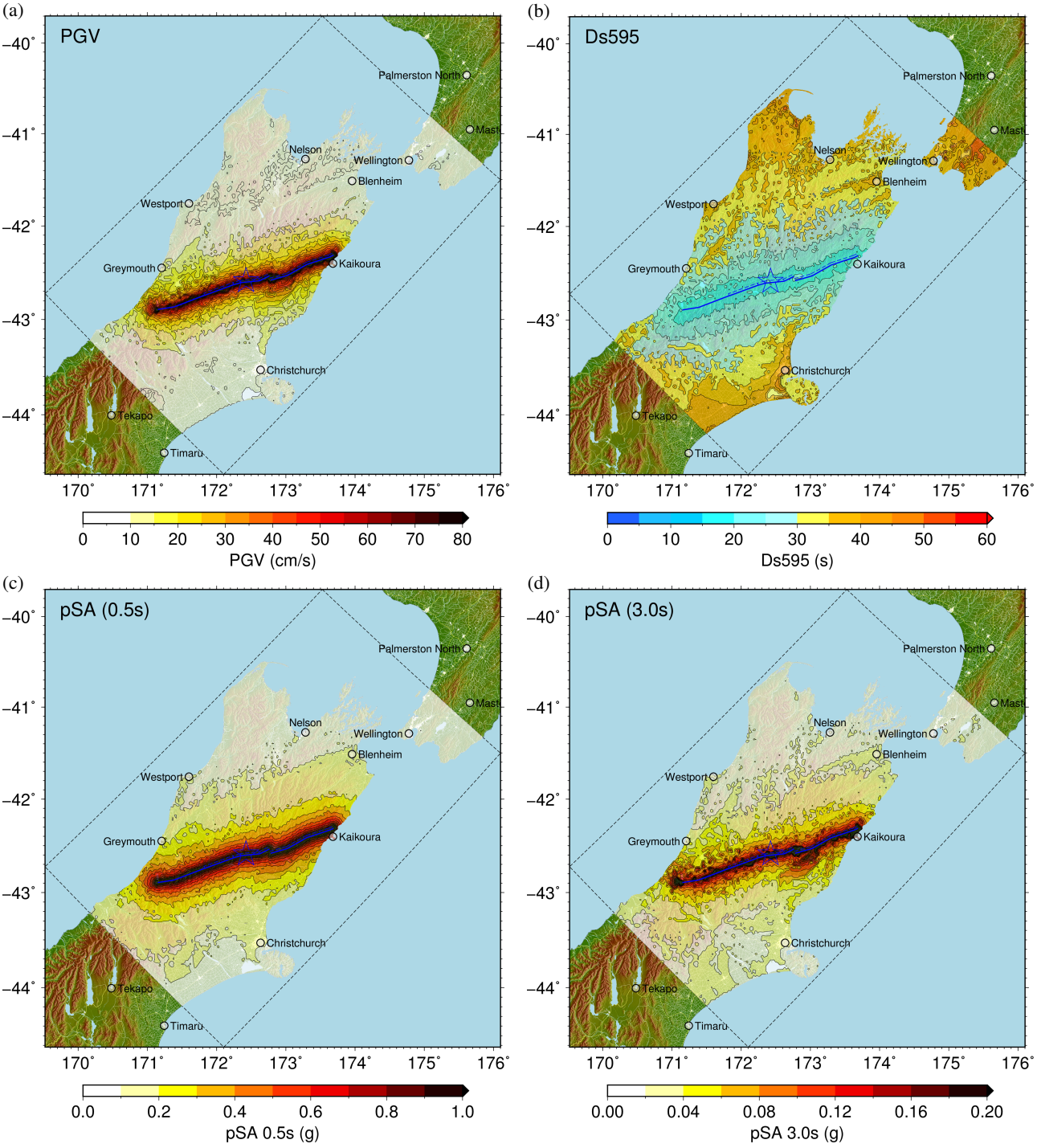

Figure 7: Empirical intensity measure estimates for the Hope Fault reference scenario: (a) PGV; (b) D_{s5-95}; (c) pSA(0.5s); and (d) pSA(3.0s). Note that a spatially-variable V_{s30} model impacts predicted values over short length scales.

$10 < R_{rup} < 80km$. For PGV, and pSA(3.0s) (Figure 9a, and Figure 9d, respectively) the effect of sedimentary basins becomes apparent as most near-source locations ($R_{rup} < 10km$) are not in modelled basins (hence simulations have lower intensities at these distances) whereas at larger distances an increasing proportion of the data are in basins and therefore, generally have higher intensities.

Sensitivity Analysis

Method and Variables

A sensitivity analysis was conducted to investigate the effect of source variations on simulated ground motions. Specific focus is given to source variability and not to path or site effects, which are by their nature, more localised in terms of influence. Only a limited number of source uncertainties are investigated, however, the specific parameters were selected because of the expectation that they have the greatest effect on simulated ground motions over the region of interest. Table 1 presents the four source quantities analysed: magnitude, stress parameter, hypocentre location and slip distribution (which incorporates rake and rise time variations, herein referred to as simply slip for brevity), and the values used for each quantity. Delays in rupture initiation and kinematic triggering between fault segments were not investigated. Only two variations considered for each parameter were investigated here as this sensitivity analysis is not intended to provide a comprehensive investigation of all

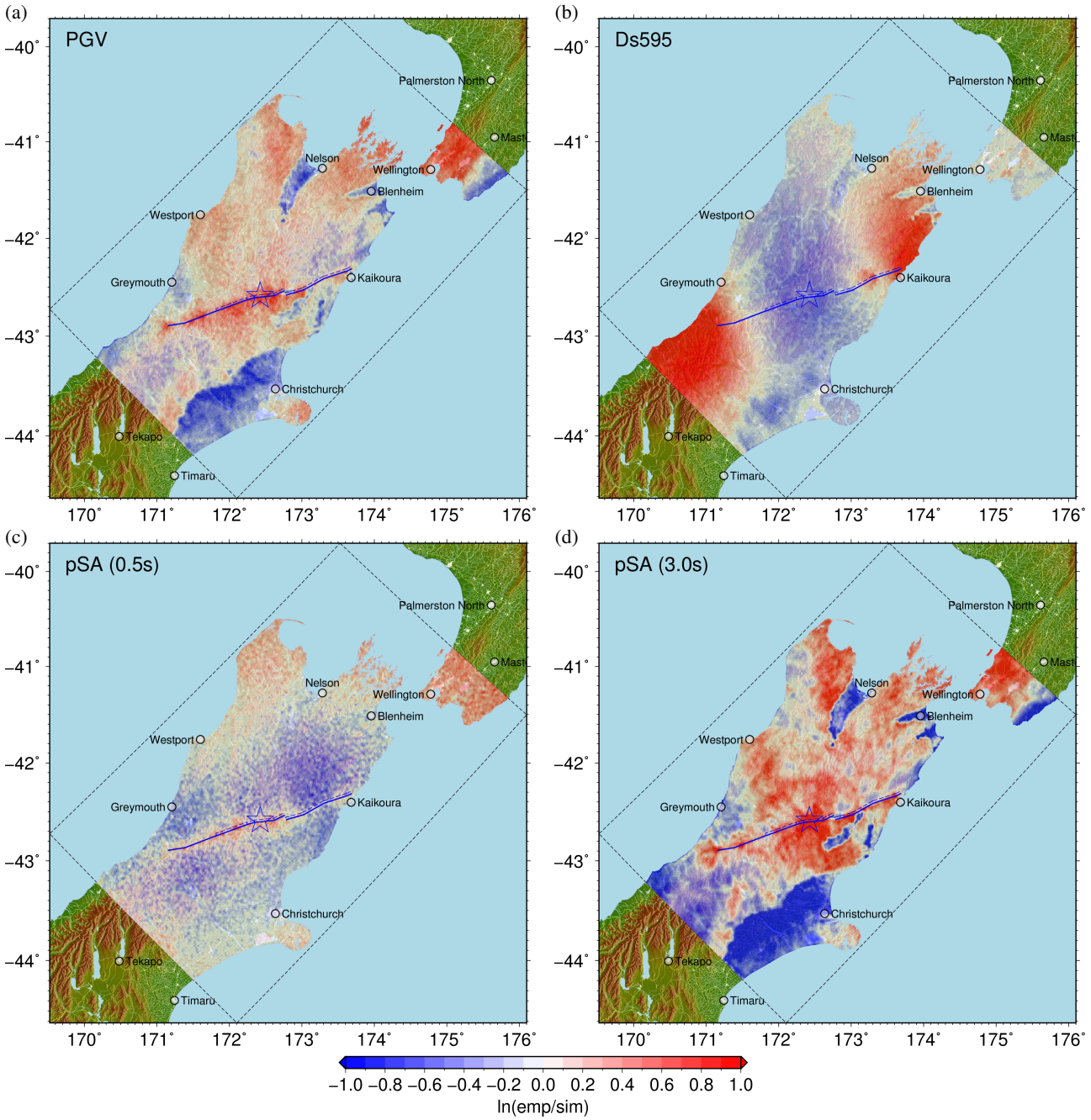

Figure 8: Ratios of simulated intensity measures for the Hope Fault reference simulation and empirical ground motion estimates: (a) PGV; (b) D_{s5-95}; (c) pSA(0.5s); and (d) pSA(3.0s).

possible rupture scenarios, instead it is intended to give insights into how the main source parameters influence simulated ground motion intensities. The general effect of varying the four source characteristics on simulations is presented in subsequent subsections (with a focus on intensity measures that best illustrate the sensitivity to each source characteristic) followed by a detailed analysis into their effect in select urban regions.

As previously noted, the magnitude estimate for the Hope Fault reference scenario was obtained via the magnitude-scaling relation of Leonard [22] which yields a median magnitude estimate of $M_w = 7.51$ and a standard deviation of 0.26. Magnitude estimates of $M_w = 7.77$ and $M_w = 7.25$ were thus utilised as representing the median plus and minus one standard deviation, respectively. Magnitude directly influences the average slip amplitude and rise time in the kinematic rupture

Table 1: Source variations explored and adopted values for sensitivity analysis.

Quantity	Variation	Values
Magnitude (M_w)	$\pm\sigma_{M_w}$	[7.25, 7.77]
Stress parameter ($\Delta\tau$) (bars)	$\pm\sigma_{ln\Delta\tau}$	[32.9, 76.1]
Hypocentre position along strike (km)	Eastern and Western hypocentres	[0, 219]
Slip distribution	Two realisations	-

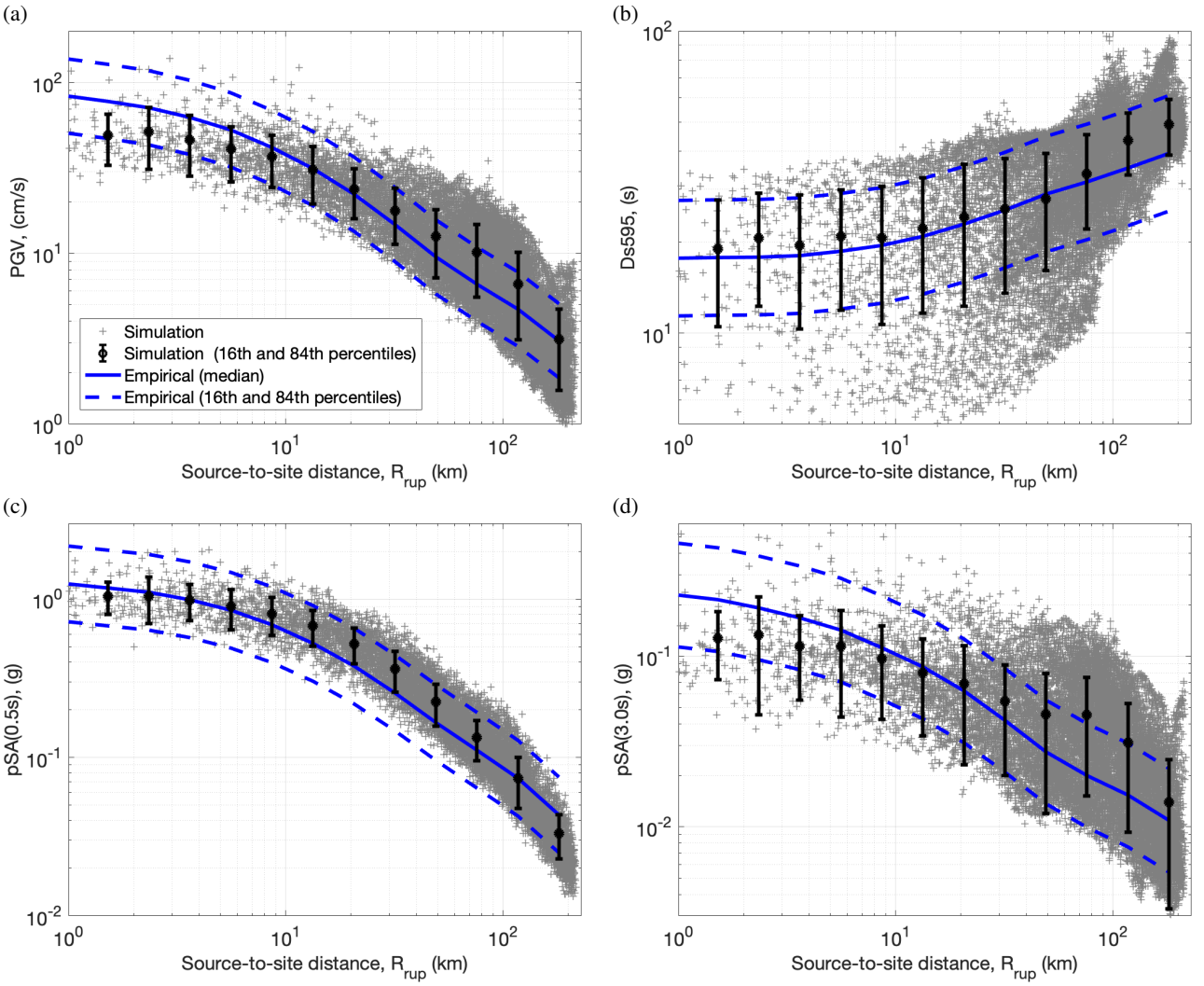

Figure 9: Comparison of empirical and simulated intensity measures as a function of R_{rup} for (a) PGV; (b) D_{s5-95}; (c) pSA(0.5s); and (d) pSA(3.0s) (error bars represent one standard deviation).

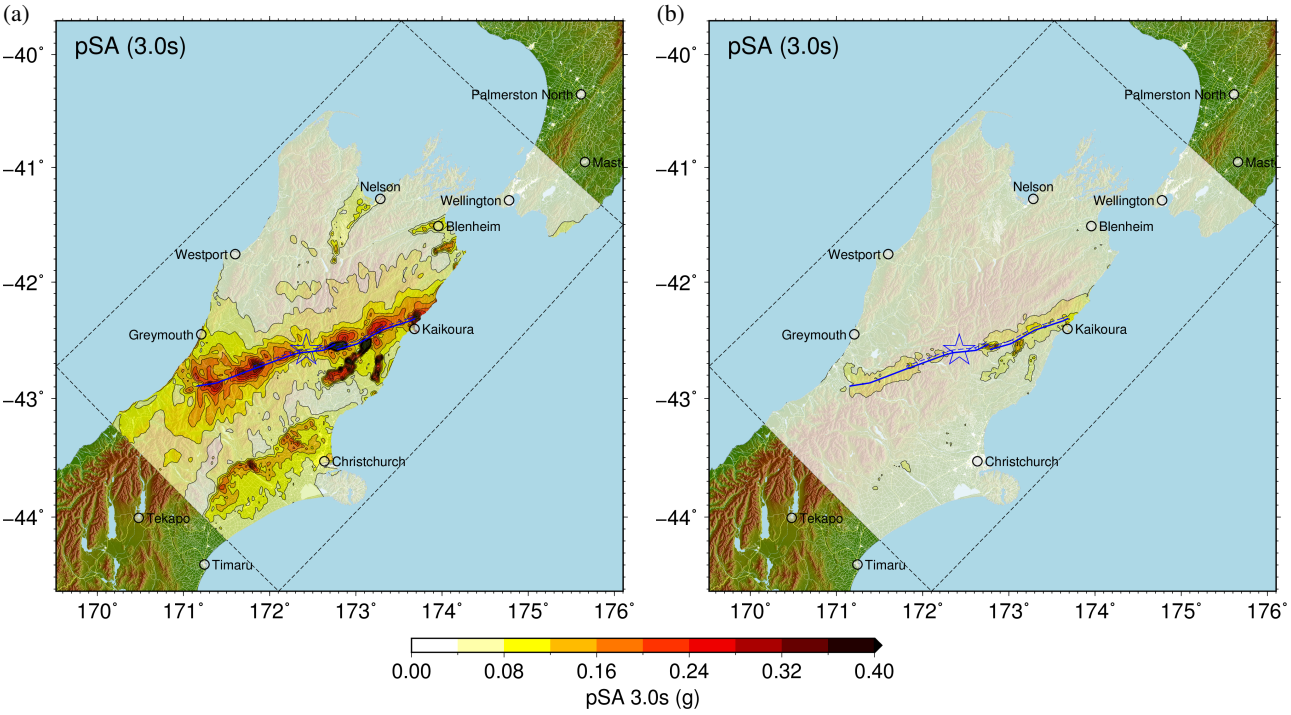

Figure 10: Effect of magnitude variability on pSA(3.0s) for: (a) upper (M_w7.77); and (b) lower (M_w7.25) magnitude estimates.

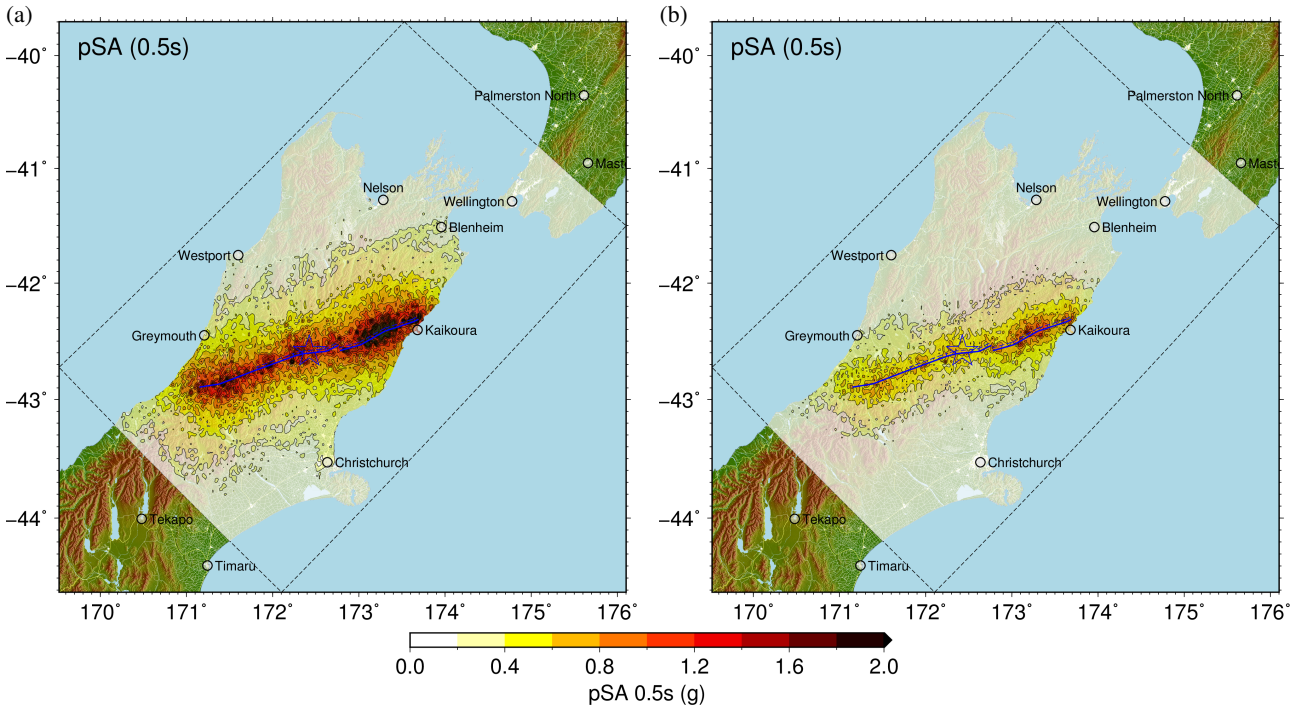

Figure 11: Effect of stress parameter variability on pSA(0.5s) for: (a) upper ($\Delta\tau = 76.1$bar); and (b) lower ($\Delta\tau = 32.9$bar) estimates.

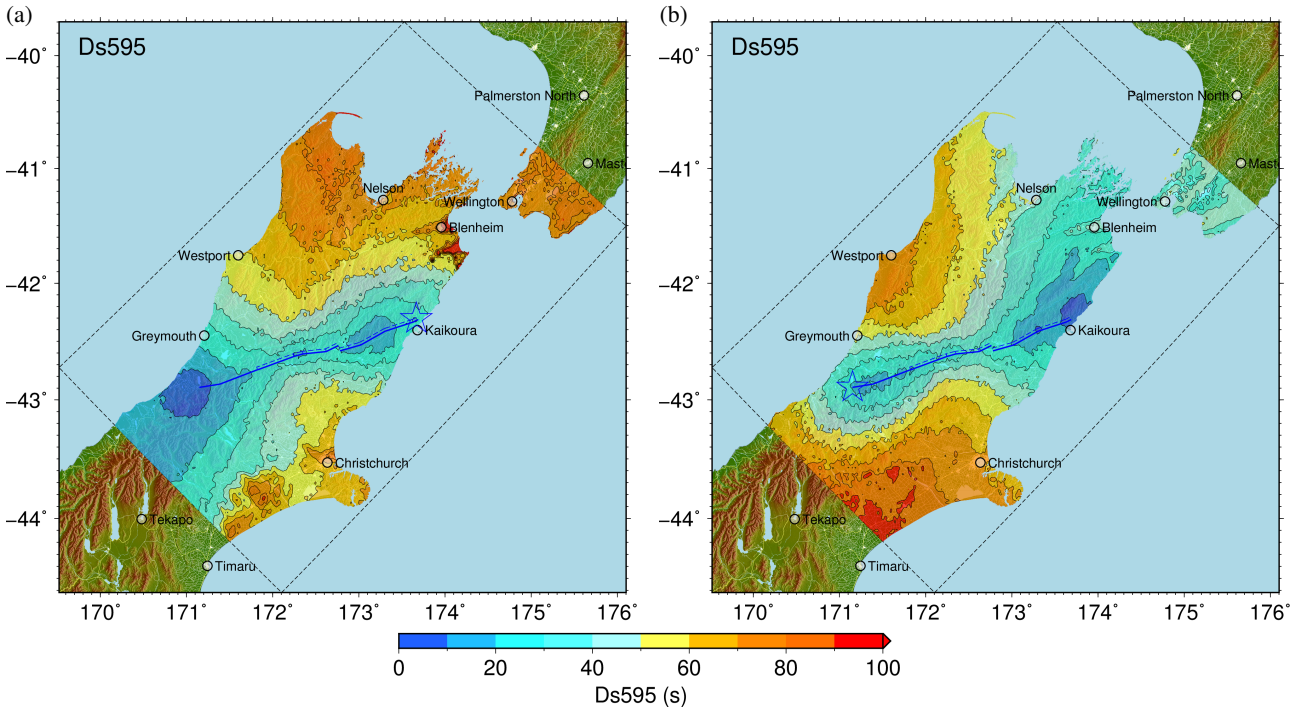

Figure 12: Effect of hypocentre location on D_{s5-95}: (a) Eastern hypocentre; and (b) Western hypocentre.

generation. For the two magnitude variations explored, the upper estimate leads to an increase in average slip on the fault surface from 108cm to 256cm, while the lower magnitude estimate decreases the average slip from 108cm to 42cm. The effect of these magnitude estimates on ground motions intensities is presented in Effect of Magnitude Variability.

In the reference Hope Fault scenario the stress parameter (also known as Brune stress drop, or static stress drop) ($\Delta\tau$) was set to 50bars. This parameter only influences the HF component of the simulation methodology [5]. Recent research (e.g. [40]) has investigated the standard deviation of the stress parameter and the inferred variability ($\sigma_{ln\Delta\tau}$), which based on the Abrahamson and Silva [41] empirical ground motion model, for a M_w7 earthquake is $\sigma_{ln\Delta\tau} = 0.42$. Simulations were conducted with the stress parameter set as 76.1bars and 32.9bars, representing the value utilised in the reference scenario plus and minus $\sigma_{ln\Delta\tau}$, respectively. Simulations varying the stress parameter are presented in Effect of Stress Parameter.

Hypocentre location is an important parameter as it highly influences ground motion directivity. The reference scenario

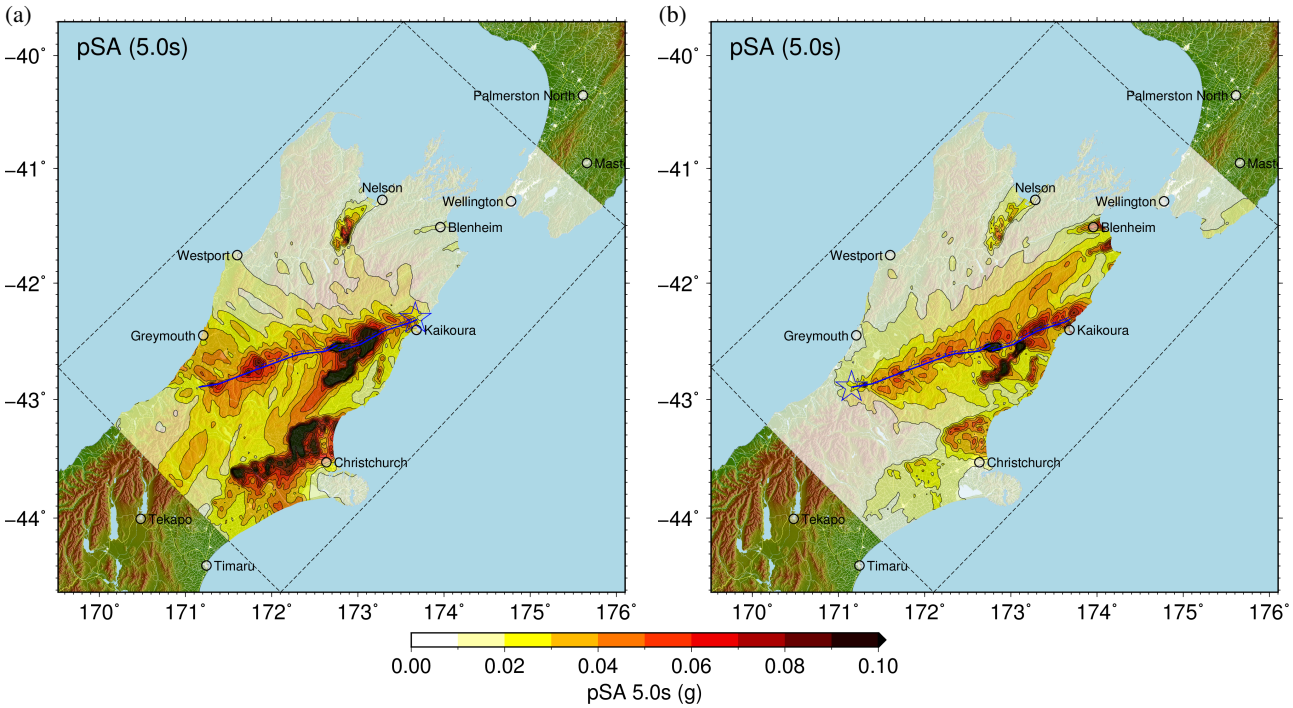

Figure 13: Effect of hypocentre location of pSA(5.0s): (a) Eastern hypocentre; and (b) Western hypocentre.

placed the hypocentre at the midpoint (109.5km) along the strike of the 219km rupture at a depth of 9km. For this analysis hypocentre locations at the Eastern and Southern extents, 0km and 219km along strike, respectively, at a depth of 9km were adopted. Simulations of these ruptures and their effect on ground motions are presented in Effect of Hypocentre Location. The depth of the hypocentre was not deemed an important factor for this sensitivity analysis relative to the effect of location along strike and therefore was not investigated.

The sensitivity to slip is investigated by considering different random realisations of the slip distribution produced by the Graves and Pitarka [5] rupture generator. As the slip on the rupture is stochastically generated, and fractal in nature, the concept of a minimum and maximum case do not fundamentally exist, although simulated intensity measures will vary between realisations. Two different slip realisations were generated and their effect on ground motions is presented in Effect of Kinematic Slip Distribution.

Effect of Magnitude Variability

Figure 10 illustrates the effect of magnitude variability (see Table 1) on pSA(3.0s). The effect is the upper magnitude estimate scenario (M_w7.77) has a higher pSA(3.0s) over the region than the lower magnitude estimate scenario (M_w7.25), as expected given an identical slip distribution pattern (albeit with a higher amplitude) and hypocentre location. Varying the magnitude in broad terms has a similar effect on all waveform amplitude intensity measures, with an increase in magnitude increasing the intensity measure and vice versa (rupture models for two magnitudes explored can be found in the appendix).

Effect of Stress Parameter

Figure 11 presents the effect of the upper ($\Delta\tau = 76.1$bar) and lower ($\Delta\tau = 32.9$bar) stress parameter estimates on pSA(0.5s). Varying the stress parameter only influences the HF portion of the Graves and Pitarka [5] simulation methodology and therefore, only has an effect on intensity measures dominated by HF ($f > 1Hz$) ground motion. Varying the stress parameter broadly influences all HF-based intensity measures in a similar way, with increasing stress parameter increasing the intensity measure and vice versa.

Effect of Hypocentre Location

Figure 12 presents the effect of hypocentre location on D_{s5-95} for the two hypocentres considered (rupture models for the two hypocentre locations considered can be found in the appendix).

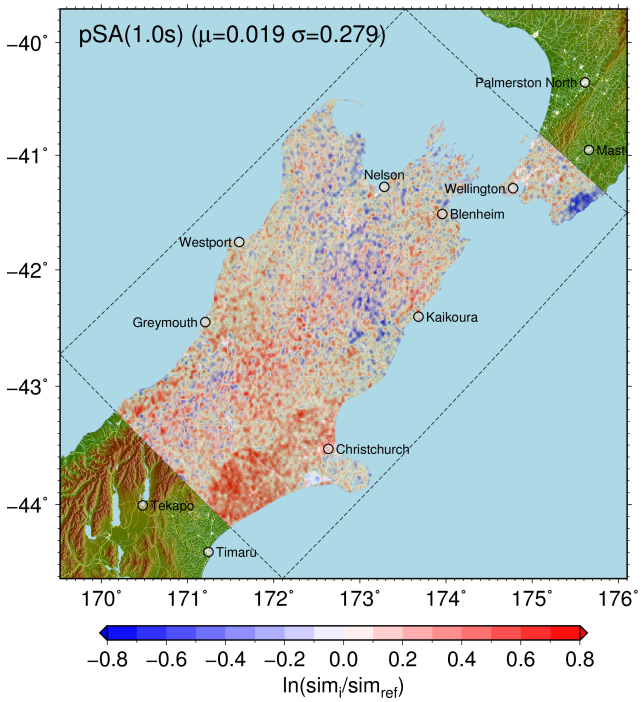

Figure 14: pSA(1.0s) ratio for two simulations with different slip realisations, with the mean (μ) and the standard deviation (σ) of the pSA(1.0s) ratio.

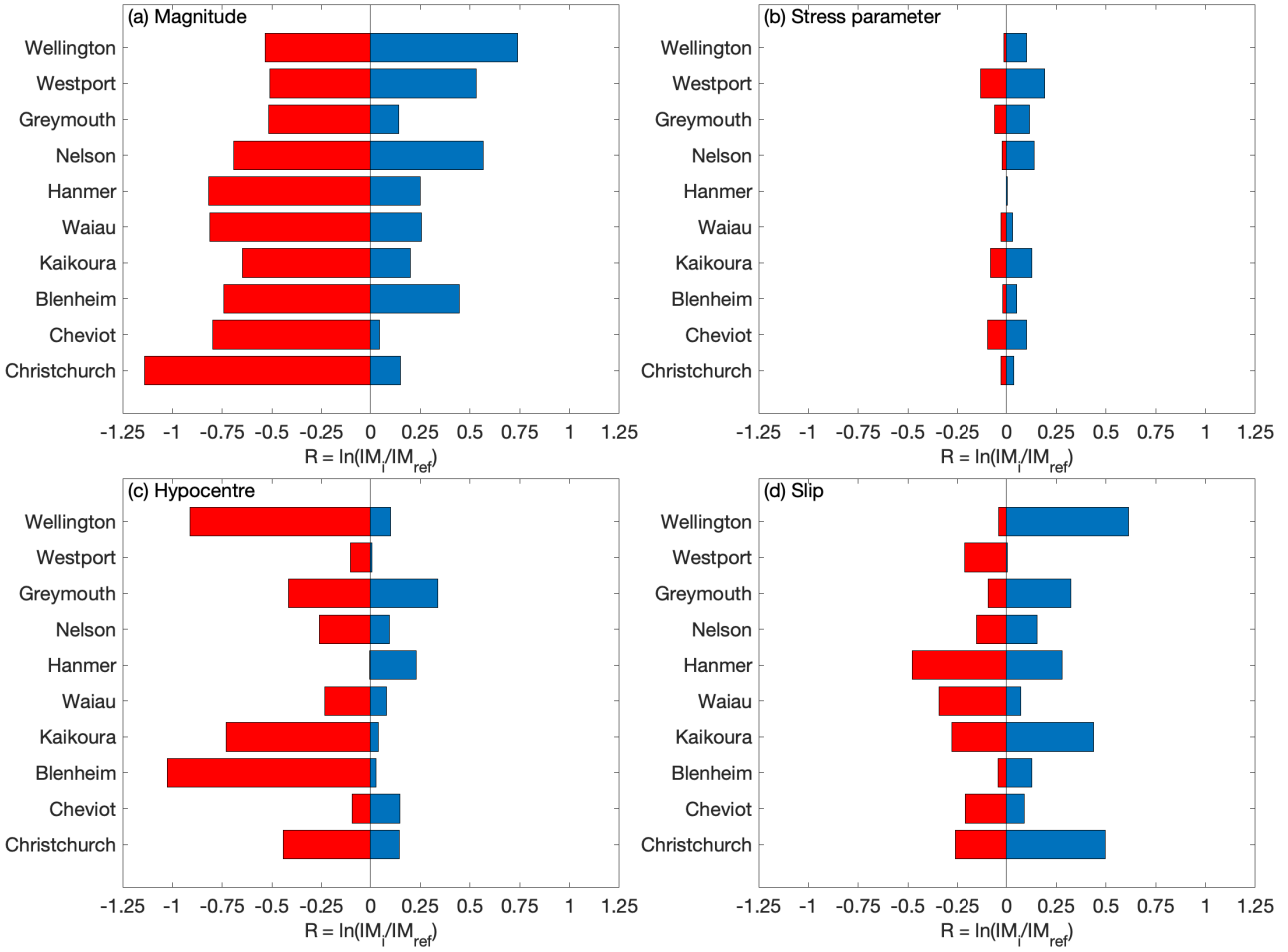

Figure 15: Effect of source variability on PGV in urban regions due to parameter variability: (a) Magnitude; (b) Stress parameter; (c) Hypocentre location; and (d) Slip distribution.

It can be seen that the Eastern hypocentre generally results in a lower duration in sedimentary basins with the exception of Canterbury, compared with the Western hypocentre scenario. Figure 13 illustrates the pSA(5.0s), for the two hypocentre cases investigated. Here the effect of rupture directivity is highly visible, as trends in pSA(5.0s) replicate the direction and spread of seismic waves propagating away from the hypocentre along the strike of the fault, with the exception of sedimentary basins which generally have a high pSA(5.0s) due to basin reverberations. (PGA for the two hypocentre locations investigated can be viewed in the appendix).

Effect of Kinematic Slip Distribution

Simulations using two sources with different slip realisations were performed (rupture models for these realisations can be found in the appendix) and Figure 14 presents pSA(1.0s) ratio of one of these simulations with the Hope Fault reference simulation. While there are local variations in the spatial distribution of pSA(1.0s) ratios (where there is roughly an equal amount of positive and negative patches), there are no significant regional trends apparent. The mean and standard deviation of the pSA(1.0s) ratios at all locations in the uniform output grid (as shown in Figure 14) are 0.019 and 0.279, respectively. The mean is effectively zero, which indicates that varying the slip can result in a local change in ground motion intensity, while over the entire simulation domain the ground motion intensity remains unchanged on average. Examination of the standard deviations of PGA, pSA(1.0s) and pSA(3.0s), which have values of 0.21, 0.27 and 0.37, respectively, suggest that standard deviation increases with vibration period (i.e. slip variability has a greater effect on longer period intensity measures).

Comparison of Parameter Sensitivities on Ground Motion Intensities in Urban Locations

Figures 15 and 16 present the effect of source variations on PGV and PGA, respectivley, at select urban regions (the locations of the specific urban regions are annotated in Figure 1). Bars were calculated as $R = \ln(IM_i/IM_{ref})$ where IM_i is the intensity measure for variation of source considered and IM_{ref} is the intensity measure for the reference simulation. Therefore, these bars represent the increase or decrease in the intensity measure with respect to the reference simulations for the source parameter considered (see Table 1). For slip and hypocentre variability the reference scenario does not necessarily produce median intensity measures. In this case, the reference intensity measure for the calculation of R is taken to be the median value.

In Figure 15 it can be seen that the effect of source parameter variations influence PGV by varying amounts at different urban regions. In broad terms, varying the magnitude estimate has the largest effect on PGV while varying the stress parameter has a relatively small effect on PGV (as expected due to PGV being a LF-dominated intensity measure). Hypocentre has the largest effect for regions in forward / backward directivity zones (e.g. Kaikōura, Blenheim, Wellington; see Figure 1) while the effect of hypocentre is relatively small for regions at large distances ($>$ 50km) perpendicular to the rupture strike direction (e.g. Nelson,

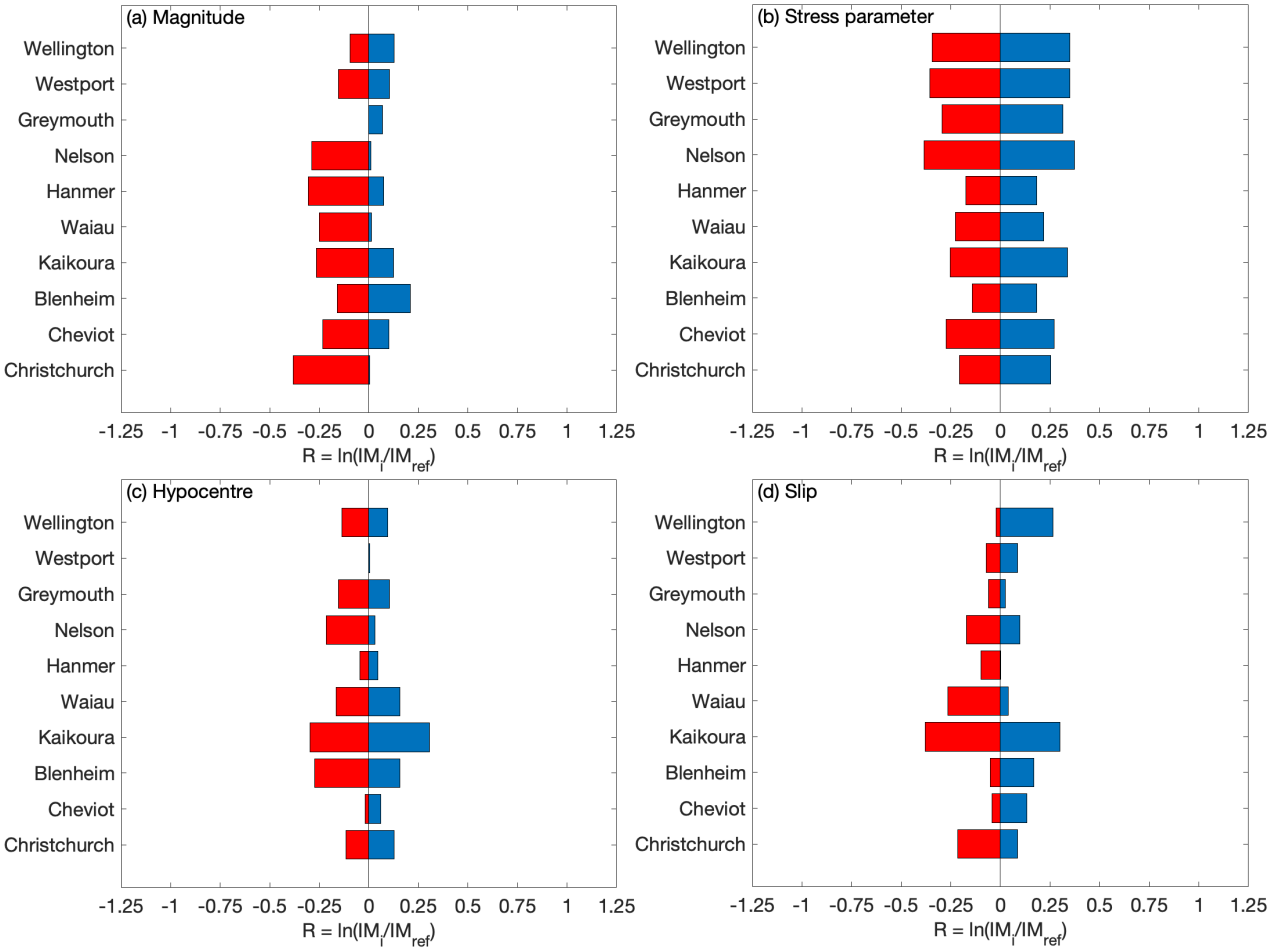

Figure 16: Effect of source variability on PGA in urban regions due to parameter variability: (a) Magnitude; (b) Stress parameter; (c) Hypocentre location; and (d) Slip distribution.

Westport) and for urban regions at small source-to-site-distances (e.g. Hanmer, Waiau, Cheviot). Slip variability had the largest effect on PGV at locations with small source-to-site distances (e.g. Hanmer and Kaikōura), due to the random locations of asperities for different slip realisations.

Figure 16 illustrates the effect of source variability on PGA. Magnitude has a less consistent influence on PGA compared with PGV, as M_w controls the corner frequency of the source spectrum in the HF method, and so has some systematic effect. However, the results show that this is less than the effect of M_w on PGV due to the spatial variation of slip amplitude (which affects the seismic moment for each subfault that comprise the total rupture). It can be seen that the stress parameter sensitivity has, on average, the largest and most consistent influence on PGA.

Comparisons with the 2016 Kaikōura Earthquake

The 2016 M_w7.8 Kaikōura earthquake was a large earthquake in the North-East of the South Island. Shaking was felt throughout the country with extensive damage observed throughout the Northern South Island and as far away as Wellington [1, 2, 42, 43]. Given the comparable magnitude of the Kaikōura earthquake (M_w7.8) with the Hope Fault scenario (M_w7.51) examined here and their close geographic locations, comparisons of ground motions with the Kaikōura earthquake can provide context to a Hope Fault scenario rupture with regard to ground motion intensities and regional impacts.

Figure 17 presents the PGV for a simulation of the 2016 Kaikōura earthquake (e.g. [1]), and the ratio of PGV of form $\ln(PGV_{Kaikoura}/PGV_{Hope})$ from the Kaikōura earthquake and the Hope Fault reference scenario previously presented in Reference Simulation. As discussed in Sensitivity Analysis, ground motions from a Hope Fault scenario vary appreciably with changes in source characteristics, here the Hope Fault reference scenario was utilised for this comparison. For the PGV ratio between these two events (Figure 17b), it can be seen that for the Northern South Island and the lower North Island that the PGV ratio is positive and we expect the shaking on average to be larger for the Kaikōura earthquake than in the Hope Fault scenario, in Canterbury and urban Christchurch the

Table 2: Comparison of simulated PGV values in urban regions for the Hope Fault reference scenario and 2016 Kaikōura Earthquake.

Urban region	PGV (cm/s)		
	Hope reference	Kaikōura	Ratio
Christchurch	15.7	16.9	0.93
Cheviot	30.9	32.1	0.96
Blenheim	13.4	58.8	0.22
Kaikōura	67.7	90.4	0.75
Waiau	75.3	69.6	1.08
Hanmer	75.8	32.3	2.35
Nelson	5.1	16.8	0.30
Greymouth	21.3	5.2	4.13
Westport	5.4	5.6	0.98
Wellington	2.3	20.8	0.11

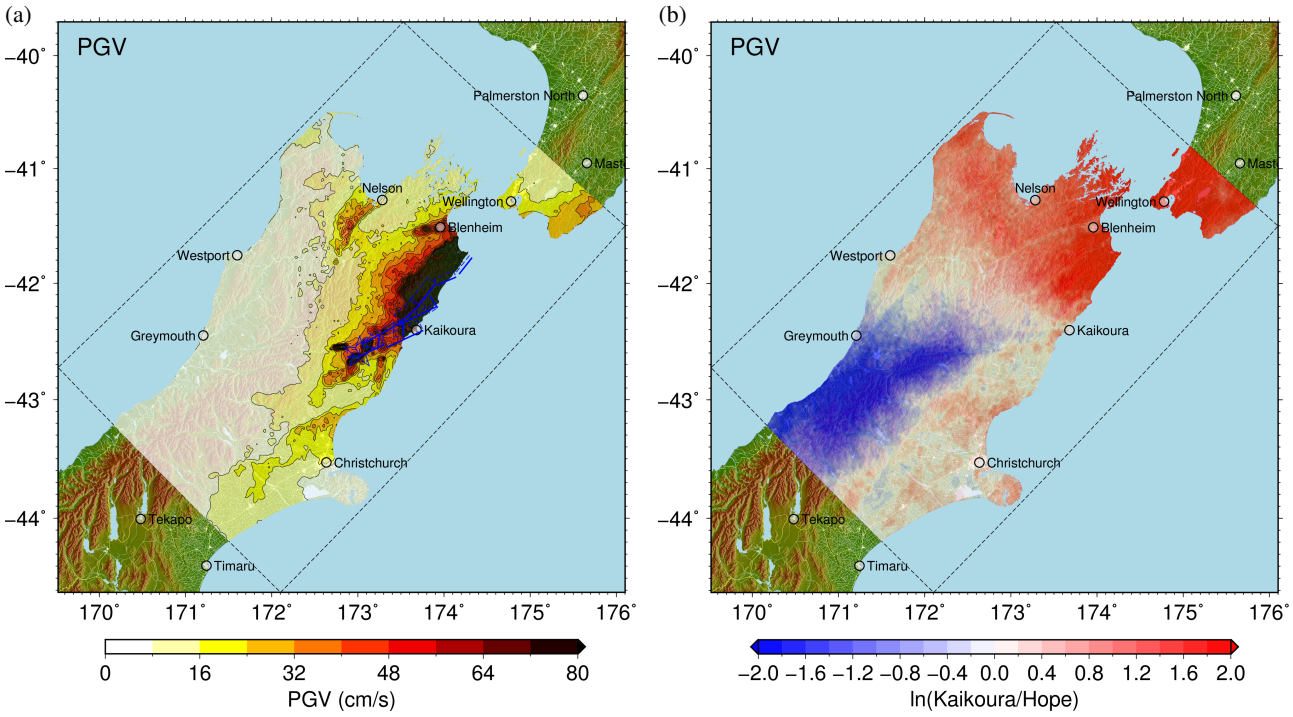

Figure 17: (a) Simulated PGV for the 2016 Kaikōura earthquake [1]; and (b) PGV ratio between the Kaikōura earthquake and Hope Fault reference scenario.

PGA is approximately the same and in the South-West of the simulation domain the PGV is larger for the Hope Fault scenario. Table 2 presents simulated PGVs and a ratio for the 2016 Kaikōura earthquake with the Hope Fault reference scenario. For the urban regions considered: Greymouth and Hanmer have significantly higher PGVs for the Kaikoura earthquake; Christchurch, Cheviot, Waiau, Kaikōura and Westport have similar PGVs for both events; while Wellington, Blenheim and Nelson have significantly lower PGVs for the Hope Fault Scenario.

Significant uncertainties regarding a Hope Fault rupture exist. There are geometric uncertainties associated with modelling the fault dimensions in addition to uncertainties regarding source modelling aspects, as explored in Sensitivity Analysis, which indicated that the ground motion amplitudes can vary appreciably due to changes in the magnitude, stress parameter, hypocentre and slip. Therefore, although the ground motion amplitudes are generally smaller in urban regions for the Hope Fault scenario presented here than the 2016 Kaikōura earthquake, additional scenarios exist where this may not be the case.

DISCUSSION AND CONCLUSIONS

This paper examined ground motions for a major rupture of the Hope Fault using a physics-based simulation methodology and a 3D crustal velocity model of New Zealand. Comparisons of simulations with conventionally utilised empirical ground motion models illustrated appreciable differences in the resulting intensity measures, particular in sedimentary basins. These basins are generally the locations of significant population centres, which are of particular interest in modelling ground motions and assessing seismic hazard. Significant validation efforts are currently underway (e.g. [25]) and are expected to provide greater confidence in the simulation-derived long-period ground motions in sedimentary basins.

The Hope Fault rupture scenario presented here is comprised of four segments from the NSHM [6], the seismic hazard from these segments are currently assessed via characteristic ruptures which excludes the possibility of rupture involving multiple segments (such as the one presented here) from occurring. Recent international research has relaxed the discrete fault assumption previously utilised to assess seismic hazard, in favour of allowing ruptures to trigger subsequent ruptures on nearby faults (e.g. [13, 44]). Further research is required to incorporate multi-fault ruptures into New Zealand seismic hazard models.

The sensitivity analysis which analysed the effect of variations in the source modelling parameters of magnitude, stress parameter, hypocentre location and kinematic slip distribution illustrated that simulated ground motion intensities can vary appreciably for different source modelling assumptions. It was found that the magnitude and stress parameter strongly influenced long and short period ground motion amplitudes, respectively. Future assessments should examine the sensitivity of ground motions to rupture geometry and variability in the 3D crustal velocity model.

The comparisons of the Hope Fault reference simulation with the 2016 Kaikōura earthquake illustrated that the PGV is expected to be lower for the Hope Fault than inferred for the Kaikōura earthquake for the majority of urban regions. However, considering the variations in source modelling explored here, in addition to other model uncertainties (e.g. fault geometry), there is the potential for the ground motions from a Hope Fault earthquake to exceed those from the 2016 Kaikōura earthquake over a wider region.

DATA AND RESOURCES

The NeSI Maui HPC cluster was utilised to conduce ground motion simulations. The repositories with simulation workflows can be viewed on Github (URL: https://github.com/ucgmsim) and the source code for the New Zealand Velocity Model can also be viewed on Github (URL: https://github.com/ucgmsim/Velocity-Model).

Earthquake source descriptions used in this study were

obtained from the GeoNet New Zealand earthquake catalogue (URL: https://github.com/GeoNet/data/tree/master/moment-tensor/) recorded ground motions were obtained from the GeoNet file transfer protocol (ftp://ftp.geonet.org.nz/strong/).

Figures were prepared using Generic Mapping Tools URL: http://gmt.soest.hawaii.edu/ [45], Python (URL: https://www.python.org/); and Matplotlib (URL: https://matplotlib.org/), [46].

A 3D ground motion simulation visualtion of the Hope Fault reference rutpure scenario can be viewed on YouTube (URL: https://youtu.be/VcLldPxVcN8).

ACKNOWLEDGEMENTS

Financial support of this research from the University of Canterbury, the Royal Society of New Zealand's Rutherford Postdoctoral Fellowship, QuakeCoRE: The NZ Centre for Earthquake Resilience, and the National Hazards Research Platform (NHRP) are greatly appreciated. High performance computing resources under the NeSI merit allocation are also greatly appreciated. The authors would also like to thank Jarg Pettinga for discussions of the geologic aspects of the Hope Fault, and the support of the QuakeCoRE Technical Platform 4 software development team. This project was (partially) supported by QuakeCoRE, a New Zealand Tertiary Education Commission-funded Centre. This is QuakeCoRE publication number 0427.

REFERENCES

1 Bradley BA, Razafindrakoto HN and Polak V (2017). "GroundMotion Observations from the 14 November 2016 M w 7.8 Kaikoura, New Zealand, Earthquake and Insights from Broadband Simulations". *Seismological Research Letters*, **88**(3): 740–756.

2 Hamling IJ, Hreinsdóttir S, Clark K, Elliott J, Liang C, Fielding E, Litchfield N, Villamor P, Wallace L, Wright TJ *et al.* (2017). "Complex multifault rupture during the 2016 Mw 7.8 Kaikōura earthquake, New Zealand". *Science*, **356**(6334).

3 Freund R (1971). *The Hope Fault, a Strike Slip Fault in New Zealand*, vol. 86. Dept. of Scientific and Industrial Research.

4 Langridge R, Campbell J, Hill N, Pere V, Pope J, Pettinga J, Estrada B and Berryman K (2003). "Paleoseismology and slip rate of the Conway Segment of the Hope Faultat Greenburn Stream, South Island, New Zealand". *Annals of Geophysics*, **46**(5).

5 Graves R and Pitarka A (2016). "Kinematic GroundMotion Simulations on Rough Faults Including Effects of 3D Stochastic Velocity Perturbations". *Bulletin of the Seismological Society of America*, **106**(5): 2136–2153.

6 Stirling M, McVerry G, Gerstenberger M, Litchfield N, Van Dissen R, Berryman K, Barnes P, Wallace L, Villamor P, Langridge R, Lamarche G, Nodder S, Reyners M, Bradley B, Rhoades D, Smith W, Nicol A, Pettinga J, Clark K and Jacobs K (2012). "National Seismic Hazard Model for New Zealand: 2010 Update". *Bulletin of the Seismological Society of America*, **102**(4): 1514–1542, DOI: 10.1785/0120110170.

7 Cowan H (1991). "The north Canterbury earthquake of September 1, 1888". *Journal of the Royal Society of New Zealand*, **21**(1): 1–12.

8 Langridge R and Berryman K (2005). "Morphology and slip rate of the Hurunui section of the Hope Fault, South Island, New Zealand". *New Zealand Journal of Geology and Geophysics*, **48**(1): 43–57.

9 Langridge R, Villamor P, Basili R, Almond P, Martinez-Diaz J and Canora C (2010). "Revised slip rates for the Alpine fault at Inchbonnie: Implications for plate boundary kinematics of South Island, New Zealand". *Lithosphere*, **2**(3): 139–152.

10 Thomson EM, Bradley BA and Lee RL (2019). "Methodology and computational implementation of a New Zealand Velocity Model (NZVM2.0) for broadband ground motion simulation". *New Zealand Journal of Geology and Geophysics*: 1–18, DOI: 10.1080/00288306.2019.1636830.

11 Van Dissen R and Yeats RS (1991). "Hope fault, Jordan thrust, and uplift of the seaward Kaikoura Range, New Zealand". *Geology*, **19**(4): 393–396.

12 Cowan H and McGlone M (1991). "Late Holocene displacements and characteristic earthquakes on the Hope River segment of the Hope Fault, New Zealand". *Journal of the Royal Society of New Zealand*, **21**(4): 373–384.

13 Field EH, Arrowsmith RJ, Biasi GP, Bird P, Dawson TE, Felzer KR, Jackson DD, Johnson KM, Jordan TH and Madden C (2014). "Uniform California earthquake rupture forecast, version 3 (UCERF3)The timeindependent model". *Bulletin of the Seismological Society of America*, **104**(3): 1122–1180.

14 Field EH, Biasi GP, Bird P, Dawson TE, Felzer KR, Jackson DD, Johnson KM, Jordan TH, Madden C and Michael AJ (2015). "Longterm timedependent probabilities for the third Uniform California Earthquake Rupture Forecast (UCERF3)". *Bulletin of the Seismological Society of America*, **105**(2A): 511–543.

15 Wesnousky SG (2006). "Predicting the endpoints of earthquake ruptures". *Nature*, **444**(7117): 358.

16 Pagli C, Pedersen R, Sigmundsson F and Feigl KL (2003). "Triggered fault slip on June 17, 2000 on the Reykjanes Peninsula, SWIceland captured by radar interferometry". *Geophysical Research Letters*, **30**(6).

17 Nissen E, Elliott J, Sloan R, Craig T, Funning G, Hutko A, Parsons B and Wright T (2016). "Limitations of rupture forecasting exposed by instantaneously triggered earthquake doublet". *Nature Geoscience*, **9**(4): 330.

18 Litchfield N, Benson A, Bischoff A, Hatem A, Barrier A, Nicol A, Wandres A, Lukovic B, Hall B and Gasston C (2016). "Preliminary surface fault displacement measurement for the14th November 2016 M7. 8 Kaikoura Earthquake. Version 2".

19 King GCP and Wesnousky SG (2007). "Scaling of fault parameters for continental strike-slip earthquakes". *Bulletin of the Seismological Society of America*, **97**(6): 1833–1840, DOI: 10.1785/0120070048.

20 Graves R and Pitarka A (2015). "Refinements to the Graves and Pitarka (2010) broadband groundmotion simulation method". *Seismological Research Letters*, **86**(1): 75–80.

21 Bradley BA, Bae SE, Polak V, Lee RL, Thomson EM and Tarbali K (2017). "Ground motion simulations of great earthquakes on the Alpine Fault: effect of hypocentre location and comparison with empirical modelling". *New Zealand Journal of Geology and Geophysics*, **60**(3): 188–198.

22 Leonard M (2014). "Selfconsistent earthquake faultscaling relations: Update and extension to stable continental strikeslip faults". *Bulletin of the Seismological Society of America*, **104**(6): 2953–2965.

23 Tarbali K, Bradley B, Huang J, Polak V, Lagrava D, Motha J

and Bae S (2018). "Cybershake NZ v17.9: New Zealand simulation-based probabilistic seismic hazard analysis". *16th European Conference on Earthquake Engineering (16ECEE), Thessaloniki, Greece.*

24 Graves R, Jordan TH, Callaghan S, Deelman E, Field E, Juve G, Kesselman C, Maechling P, Mehta G, Milner K, Okaya D, Small P and Vahi K (2011). "CyberShake: A Physics-Based Seismic Hazard Model for Southern California". *Pure and Applied Geophysics*, **168**(3): 367–381, DOI: 10.1007/s00024-010-0161-6.

25 Lee RL, Bradley BA, Stafford PJ, Graves RW and Rodriguez-Marek A (2019). "Hybrid Broadband Ground Motion Simulation Validation of Small Magnitude Earthquakes in Canterbury, New Zealand". *Earthquake Spectra (in press)*.

26 Bradley B, Jeong S and Razafindrakoto H (2015). "Validation of empirical and physics-based ground motion and site response prediction models for the 2010-2011 Canterbury earthquakes". *Proceedings of 6th International Conference on Earthquake Geotechnical Engineering, Christchurch, New Zealand*.

27 Razafindrakoto HN, Bradley BA and Graves RW (2018). "Broadband Ground-Motion Simulation of the 2011 M w 6.2 Christchurch, New Zealand, Earthquake". *Bulletin of the Seismological Society of America*, **108**(4): 2130–2147.

28 Graves RW and Pitarka A (2010). "Broadband Ground-Motion Simulation Using a Hybrid Approach". *Bulletin of the Seismological Society of America*, **100**(5a): 2095–2123, DOI: 10.1785/0120100057.

29 Campbell KW and Bozorgnia Y (2014). "NGA-West2 Ground Motion Model for the Average Horizontal Components of PGA, PGV, and 5% Damped Linear Acceleration Response Spectra". *Earthquake Spectra*, **30**(3): 1087–1115, DOI: 10.1193/062913eqs175m.

30 Foster K, Bradley B, McGann C and Wotherspoon L (2019). "A Vs30 Map for New Zealand based on Geologic and Terrain Proxy Variables and Field Measurements". *Earthquake Spectra In-Press*, DOI: 10.1193/121118EQS281M.

31 Douglas J and Boore DM (2011). "High-frequency filtering of strong-motion records". *Bulletin of Earthquake Engineering*, **9**(2): 395–409.

32 Bradley BA (2018). "On-going challenges in physics-based ground motion prediction and insights from the 20102011 Canterbury and 2016 Kaikoura, New Zealand earthquakes". *Soil Dynamics and Earthquake Engineering*, DOI: https://doi.org/10.1016/j.soildyn.2018.04.042.

33 Aagaard BT, Brocher TM, Dolenc D, Dreger D, Graves RW, Harmsen S, Hartzell S, Larsen S and Zoback ML (2008). "Ground-motion modeling of the 1906 San Francisco earthquake, part I: Validation using the 1989 Loma Prieta earthquake". *Bulletin of the Seismological Society of America*, **98**(2): 989–1011, DOI: 10.1785/0120060409.

34 Graves RW, Aagaard BT and Hudnut KW (2011). "The ShakeOut Earthquake Source and Ground Motion Simulations". *Earthquake Spectra*, **27**(2): 273–291, DOI: 10.1193/1.3570677.

35 Bradley BA, Pettinga D, Baker JW and Fraser J (2017). "Guidance on the Utilization of Earthquake-Induced Ground Motion Simulations in Engineering Practice". *Earthquake Spectra*, **33**(3): 809–835, DOI: 10.1193/120216eqs219ep.

36 Taborda R, Azizzadeh-Roodpish S, Khoshnevis N and Cheng K (2016). "Evaluation of the southern California seismic velocity models through simulation of recorded events". *Geophysical Journal International*, **205**(3): 1342–1364.

37 Bradley BA (2013). "A New Zealand-specific pseudospectral acceleration groundmotion prediction equation for active shallow crustal earthquakes based on foreign models". *Bulletin of the Seismological Society of America*, **103**(3): 1801–1822.

38 Bellagamba X, Lee R and Bradley BA (2019). "A neural network for automated quality screening of ground motion records from small magnitude earthquakes". *Earthquake Spectra (preprint)*, DOI: 10.1193/122118EQS292M.

39 Afshari K and Stewart JP (2016). "Physically parameterized prediction equations for significant duration in active crustal regions". *Earthquake Spectra*, **32**(4): 2057–2081.

40 Cotton F, Archuleta R and Causse M (2013). "What is sigma of the stress drop?" *Seismological Research Letters*, **84**(1): 42–48.

41 Abrahamson N and Silva W (2008). "Summary of the Abrahamson & Silva NGA ground-motion relations". *Earthquake Spectra*, **24**(1): 67–97.

42 Kaiser A, Balfour N, Fry B, Holden C, Litchfield N, Gerstenberger M, DAnastasio E, Horspool N, McVerry G and Ristau J (2017). "The 2016 Kaikoura, New Zealand, earthquake: preliminary seismological report". *Seismological Research Letters*, **88**(3): 727–739.

43 Bradley BA, Wotherspoon LM and Kaiser AE (2017). "Ground motion and site effect observations in the Wellington region from the 2016 Mw 7.8 Kaikoura, New Zealand, earthquake". *Bulletin New Zealand Society Earthquake Engineering*, **50**(2): 94–105.

44 Richards-Dinger K and Dieterich JH (2012). "RSQSim earthquake simulator". *Seismological Research Letters*, **83**(6): 983–990.

45 Wessel P and Smith WH (1998). "New, improved version of Generic Mapping Tools released". *Eos, Transactions American Geophysical Union*, **79**(47): 579–579.

46 Hunter JD (2007). "Matplotlib: A 2D graphics environment". *Computing in Science & Engineering*, **9**(3): 90.

APPENDICES

Validation Events

Table 3: Validation event characteristics and number of high quality ground motion records utilised.

GeoNet Event ID	Magnitude (M_w)	Number of records utilised
2017p124453	4.0	2
2016p861251	4.7	11
2017p029455	4.1	2
2252479	4.7	8
2016p872063	4.4	8
2016p859336	4.8	9
2017p795065	5.0	13

Rupture models

Models Used to Assess Hypocentre Variability

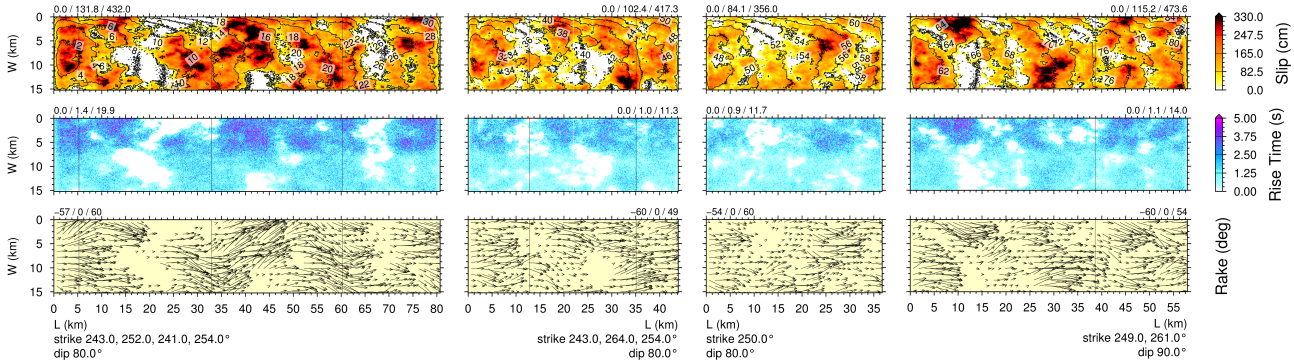

Figure 18: Eastern hypocentre source.

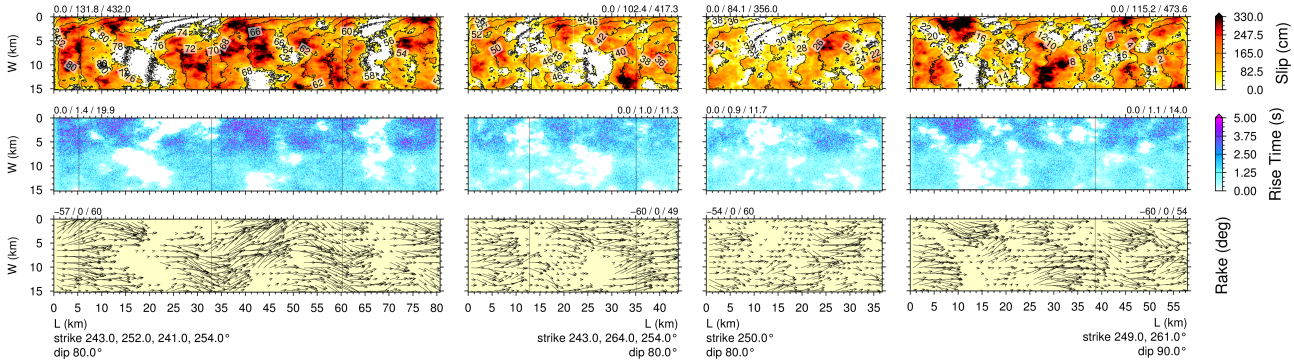

Figure 19: Western hypocentre source.

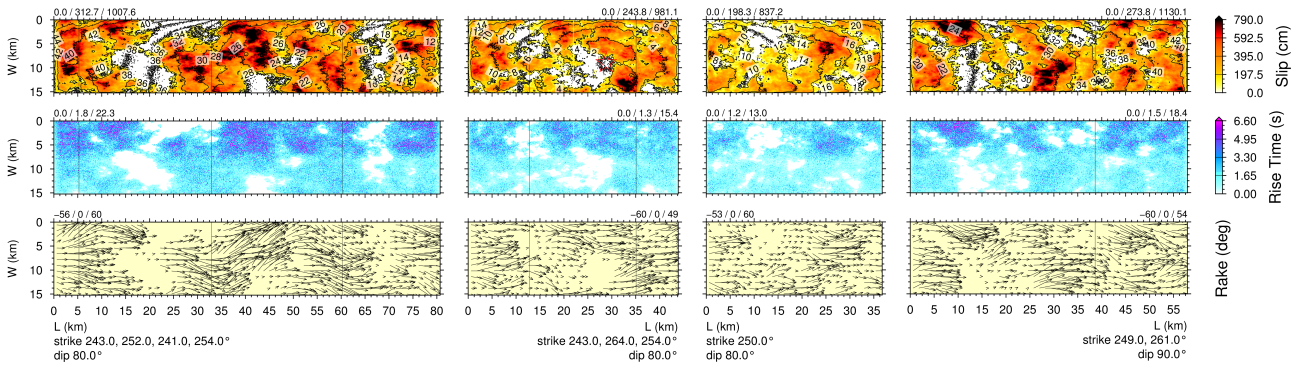

Figure 20: $+\sigma$ M_w7.77 ***magnitude source.***

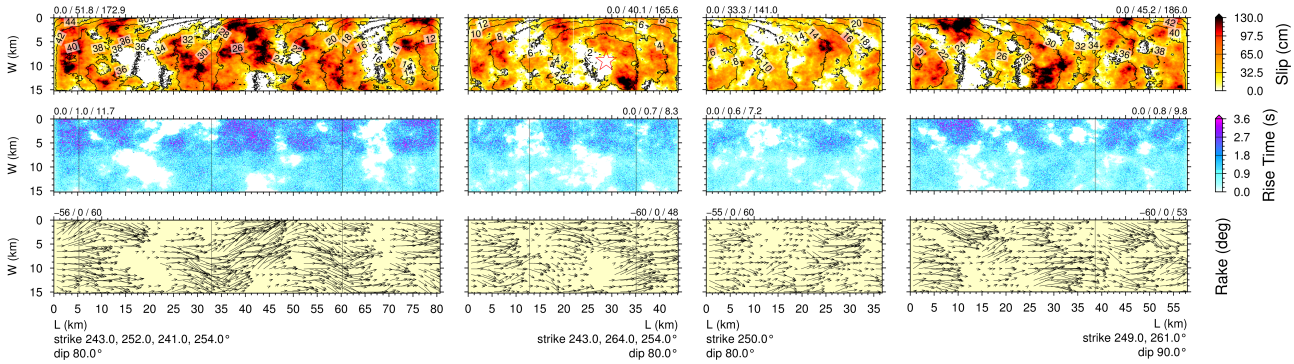

Figure 21: $-\sigma$ M_w7.25 ***magnitude source.***

Models Used to Assess Slip Variability

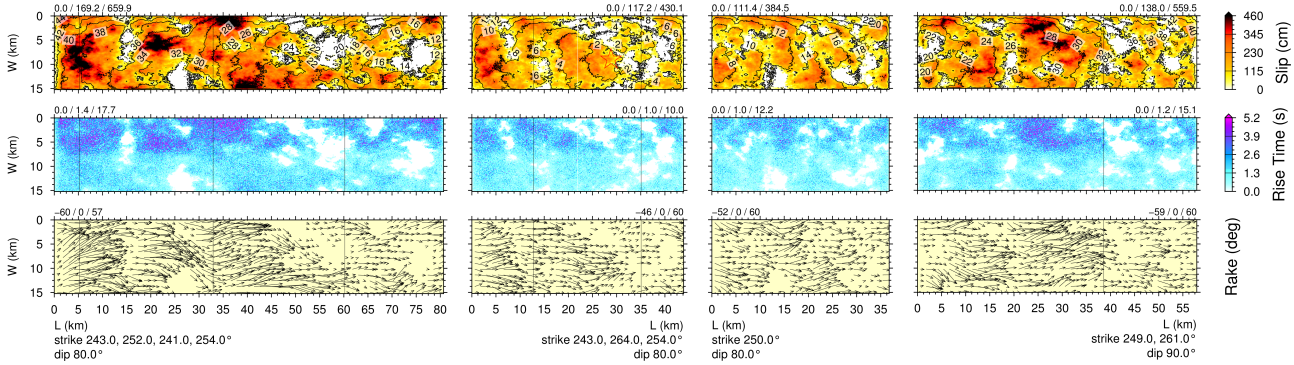

Figure 22: Slip variation A.

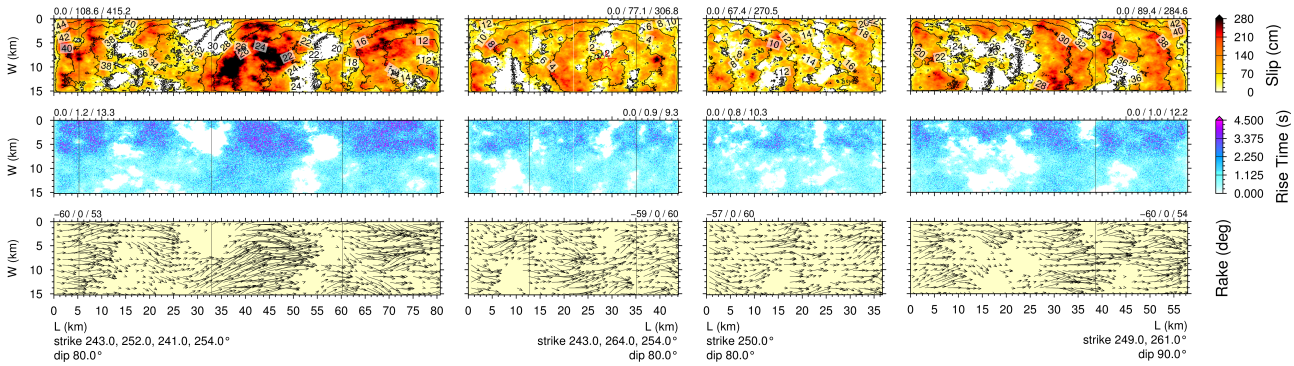

Figure 23: Slip variation B.

Hope Fault Scenario PGA Maps

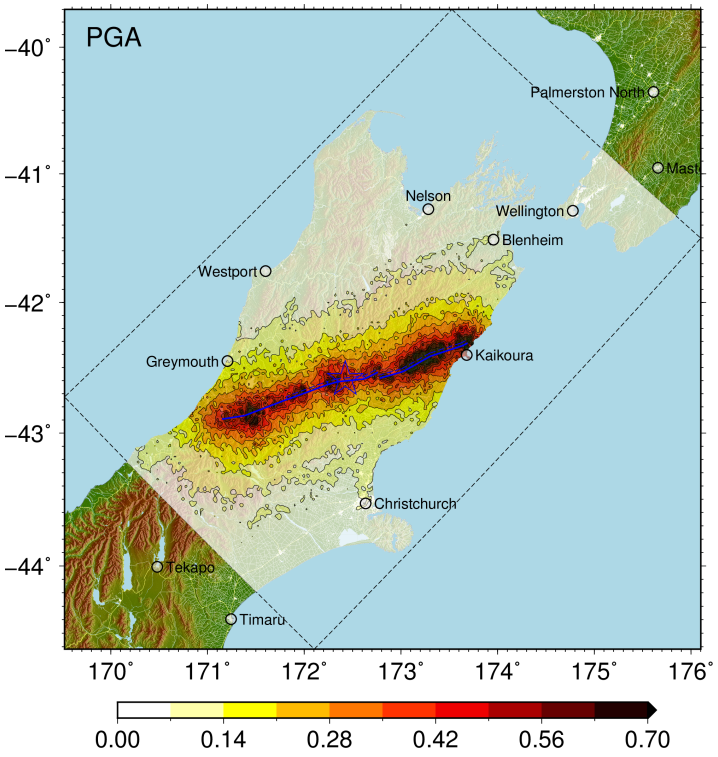

Figure 24: PGA for the Hope Fault reference scenario (units in g).

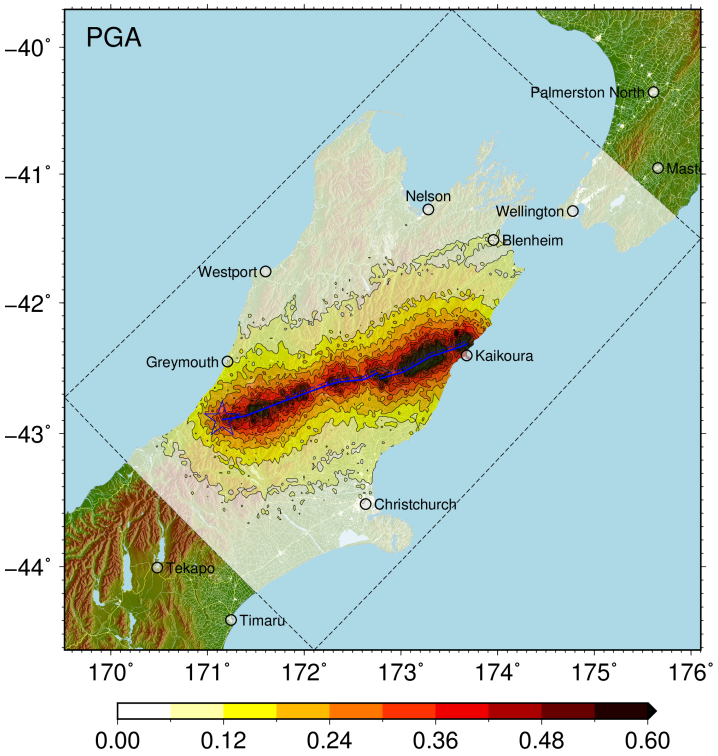

Figure 25: PGA for the Western hypocentre Hope Fault scenario (units in g).

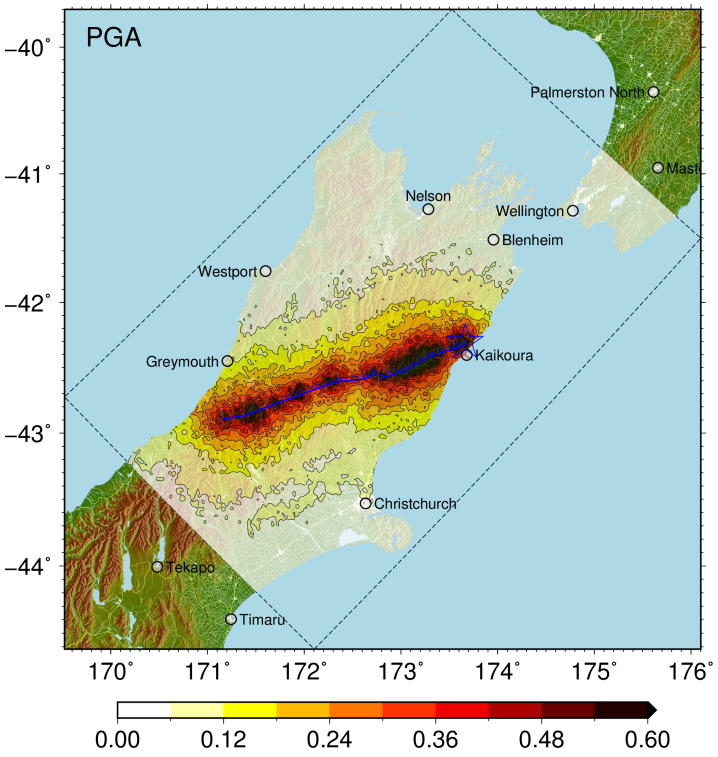

Figure 26: PGA for the Eastern hypocentre Hope Fault scenario (units in g).